Continuation for thin film hydrodynamics and related scalar problems

S. Engelnkemper, S. V. Gurevich, H. Uecker, D. Wetzel, U. Thiele

August 8, 2018

Abstract

This chapter illustrates how to apply continuation techniques in the analysis of a particular class of nonlinear kinetic equations that describe the time evolution of a single scalar field like a density or interface profiles of various types. We first systematically introduce these equations as gradient dynamics combining mass-conserving and nonmass-conserving fluxes followed by a discussion of nonvariational amendmends and a brief introduction to their analysis by numerical continuation.

The approach is first applied to a number of common examples of variational equations, namely, Allen-Cahn- and Cahn-Hilliard-type equations including certain thin-film equations for partially wetting liquids on homogeneous and heterogeneous substrates as well as Swift-Hohenberg and Phase-Field-Crystal equations. Second we consider nonvariational examples as the Kuramoto-Sivashinsky equation, convective Allen-Cahn and Cahn-Hilliard equations and thin-film equations describing stationary sliding drops and a transversal front instability in a dip-coating.

Through the different examples we illustrate how to employ the numerical tools provided by the packages AUTO07P and PDE2PATH to determine steady, stationary and time-periodic solutions in one and two dimensions and the resulting bifurcation diagrams. The incorporation of boundary conditions and integral side conditions is also discussed as well as problem-specific implementation issues.

1   Introduction

The techniques of path-continuation are widely employed to obtain branches of different types of solutions to nonlinear equations and, in consequence, to numerically construct bifurcation diagrams [4, 73, 75]. A classical, quite versatile, often used package is AUTO07P. It implements pseudo-arclength continuation algorithms and uses a discretization in the time domain (for time-periodic solutions and boundary value problems) based on orthogonal collocation employing piecewise

polynomials with a small number of collocation points per interval of the adaptive mesh [38]. In this way, the package covers most problems encountered for systems of ordinary differential equations (ODE) [36, 37] and has in some cases also been used for selected partial differential equation (PDE) or integro-differential equation (IDE) problems [13, 71, 99].

However, user-friendly tools to systematically apply continuation techniques to PDE problems are still scarce. One recently developed example is PDE2PATH, like AUTO07P using arclength continuation, but aiming at systems of PDEs in 1d, 2d and 3d, with the spatial discretization based on finite elements (FEM). See also §2 for a brief review of arclength continuation and further comments on available packages.

For spatially extended systems, e.g., described by evolution equations for concentrations, densities or interface positions the issue of symmetries and additional constraints like mass conservation becomes important as they imply that additional side conditions have to be imposed on the continuation path. This is well possible in both, AUTO07P and PDE2PATH, and normally results in additional continuation parameters besides the main one.

Here, we illustrate how to apply continuation techniques in the analysis of the solution behavior of a particular class of nonlinear kinetic equations that describe the time evolution of a single scalar field $\phi(\mathbf{r},t)$ by the action of mass-conserving fluxes $\mathbf{j}_c$ and nonmass-conserving fluxes (or rates) j_{nc}, i.e.,

$$\partial_t \phi = -\nabla \cdot \mathbf{j}_c + j_{nc}, \tag{1}$$

where ϕ might, e.g., be a density, concentration or film height, and "mass" is given by $m = \int \phi \, d^n r$ for n spatial dimensions. In many cases we first search steady solutions of (1), fulfilling

$$0 = -\nabla \cdot \mathbf{j}_c + j_{nc}. \tag{2}$$

Note that all our equations are given in nondimensional form. However, sometimes we keep nondimensional parameters that could be eliminated by scaling in order to better keep track of the individual terms. Transport equations such as (1) often describe the time evolution of density and interface profiles of various types. In many cases, the fluxes can be written in gradient dynamics (or "variational") form. In the treated case of a single scalar field ϕ, such mass-conserving and nonmass-conserving variational fluxes are given by

$$\mathbf{j}_c^g = -Q_c \nabla \mu^g = -Q_c \nabla \frac{\delta \mathscr{F}[\phi]}{\delta \phi} \quad \text{and} \quad j_{nc}^g = -Q_{nc} \mu^g = -Q_{nc} \frac{\delta \mathscr{F}[\phi]}{\delta \phi}, \tag{3}$$

respectively, i.e., Eq. (1) becomes

$$\partial_t \phi = \nabla \cdot \left[Q_c \nabla \frac{\delta \mathscr{F}[\phi]}{\delta \phi} \right] - Q_{nc} \frac{\delta \mathscr{F}[\phi]}{\delta \phi}. \tag{4}$$

Here, $\mathscr{F}[\phi]$ is an appropriately defined energy functional (here we request that it is bounded from below, i.e., exclude terms like $x\phi^n$ - but cf. Ref. [46]) and the variational derivative $\mu^g = \delta \mathscr{F}/\delta \phi$ normally corresponds to a chemical potential or pressure. The Q_i are positive definite mobility functions. Without additional nongradient terms, $\mathscr{F}$ corresponds to a Lyapunov functional for the dynamics as $d\mathscr{F}/dt \leq 0$ [120].

The simplest such equation where a spatial structure evolves is the diffusion equation – a conserved gradient dynamics where $\mathscr{F}$ is the purely entropic free

2

energy and $Q_c \sim \phi$ [41]. As it is linear and only has a homogeneous steady state, we do not consider it here. A related equation with nontrivial steady states is the Allen-Cahn (AC) equation that represents a nonconserved gradient dynamics [Eq. (4) with $Q_c = 0$] with

$$\mathscr{F}[\phi] = \int \left[\frac{\sigma}{2} (\nabla \phi)^2 + f(\phi) \right] dV \tag{5}$$

where $f(\phi)$ is a local energy function that only depends on the field itself but not on its derivatives. It is often a cubic or quartic polynomial. Furthermore, $\sigma > 0$ is a stabilizing interface stiffness, e.g., penalizes strong concentration gradients.

The AC equation can describe ordering dynamics related to a structural phase transition (e.g., the coarsening kinetics of crystal grains in alloys [3]), or simple one-component reaction-diffusion systems. Depending on the type of polynomial and scientific lineage, other names for this equation are Nagumo equation, Fisher equation, Kolmogorov-Petrovsky-Piskunov (KPP) equation, Fisher-Kolmogorov equation or Fisher-KPP equation [37, 101]. Note that for complex ϕ it is equivalent to the Ginzburg-Landau equation.

Employing the energy functional (5) in a conserved gradient dynamics [Eq. (4) with $Q_{nc} = 0$] with f being a quartic polynomial gives the Cahn-Hilliard (CH) equation that describes e.g. the decomposition dynamics of a binary mixture [22, 21]. Steady states of AC and CH equations are related as discussed more in detail in section 3. Note that the thin-film (TF) equation describing the dewetting of a liquid thin film or droplet coarsening on a horizontal solid substrate [94, 119, 12, 120] also corresponds to such a conserved gradient dynamics with a nonlinear (cubic) Q_c and particular functions $f(\phi)$ representing various wetting potentials [86, 109, 96, 126].

The square-gradient term in the energy (5) penalizes interfaces and acts stabilizing in AC and CH dynamics. It can also have a negative prefactor and then promotes interface formation. In this case, normally, a higher order term acts stabilizing. The simplest corresponding energy functional has the form

$$\mathscr{F}[\phi] = \int \left[\frac{\kappa}{2} (\Delta \phi)^2 - \frac{\sigma}{2} (\nabla \phi)^2 + f(\phi) \right] dV \tag{6}$$

where, in addition to eq. (5), $\kappa > 0$ represents the energetic cost of corners in the profile, and $f(\phi)$ is a local free energy as above.

A nonconserved gradient dynamics on the energy functional (6) is the Swift-Hohenberg (SH) equation that is the typical model equation for the dynamics of pattern formation close to the threshold of a short-scale instability [28]. It is usually applied with $f(\phi)$ being a polynomial up to sixth order [102, 19, 8, 82]. Employing the energy functional (6) in a conserved gradient dynamics gives the Phase-Field-Crystal (PFC) equation [43, 44] (also called conserved Swift-Hohenberg (cSH) equation [123]) that describes e.g. the microscopic crystallization dynamics of a colloidal suspension on diffusive timescales [7] and is also extensively used in material science [43, 127, 44]. Steady states of SH and PFC equations are discussed in more detail in section 4.

Note that there exist many more kinetic equations of the form (1). Here, we only mention classical Dynamical Density Functional Theories (DDFT) describing the behavior of colloidal systems [83, 6, 44]. They normally correspond to a conserved dynamics ($Q_{nc} = 0$) with a functional $\mathscr{F}[\phi]$ that contains nonlocal kernels. Then Eq.(4) corresponds to an integro-differential equation (IDE).

The study of nongradient variants of all the introduced equations is widespread, but to our knowledge no overall systematics has been worked out. In such equations both fluxes in Eq. (1) are sums of a gradient dynamics (or "variational") term as given in (3) and a nongradient dynamics ("nonvariational") term. In the context of Eq. (4) the nonvariational contribution typically takes three forms as summarized in the general evolution equation

$$\partial_t \phi = \nabla \cdot \left[Q_c \nabla \left(\frac{\delta \mathscr{F}[\phi]}{\delta \phi} + \mu_c^{\mathrm{ng}} \right) - \mathbf{j}_c^{\mathrm{ng}} \right] - \left(Q_{nc} \frac{\delta \mathscr{F}[\phi]}{\delta \phi} + \mu_{nc}^{\mathrm{ng}} \right). \quad (7)$$

These nongradient contributions are related to (i) an additional nonequilibrium chemical potential μ_c^{ng} in the conserved dynamics, (ii) an additional flux $\mathbf{j}_c^{\mathrm{ng}}$ generated by an additional driving force that can not be written as the gradient of a chemical potential, and (iii) a nonequilibrium chemical potential μ_{nc}^{ng} in the nonconserved dynamics.

(i) The first type are additions μ_c^{ng} to the chemical potential in the mass-conserving contribution that can not be obtained by a variation of an energy functional. Up to second order they are of the form $(1-\tilde{\beta})\frac{v'(\phi)}{2}|\nabla\phi|^2 + (1+\beta)v(\phi)\Delta\phi$ where $v(\phi)$ is some function. It is nonvariational for all $\beta, \tilde{\beta} \neq 0$ (that may depend on ϕ). For the Cahn-Hilliard equation, common choices are $\beta = \tilde{\beta} = -1$ [140, 23] and $\beta = \tilde{\beta} = 1$ [116].

(ii) The second type are additions $\mathbf{j}_c^{\mathrm{ng}}$ to the mass-conserving flux that break the isotropy (in 1d parity) of the system and correspond to lateral driving forces. Typical contributions are of the form $(\phi^n, 0)^T$ with n being some integer. For instance, $n = 1$ results in a driving comoving frame term relevant e.g. in dragged-plate studies of Landau-Levich type (TF equation) or descriptions of Langmuir-Blodgett transfer of surfactant molecules onto a moving plate (convective CH equation) [51, 71] or for driven pinned atomic monolayers (PFC, [1]) or clusters (DDFT, [99]); $n = 2$ is used in another convective CH equation [54], in the Kuramoto-Sivashinsky (KS) equation [62], (dissipative) Burgers equation [50], and liquid films driven by a thermal gradient [88]; and $n = 3$ occurs in the thin-film equation for sliding drops or film flow on an incline [112, 46]. Other terms are dispersion contributions $\partial_{xx}\phi$ added to the flux in one-dimensional KS equations [2].

(iii) Also nonconserved nongradient terms μ_{nc}^{ng} may be added to a mass-conserving dynamics. For instance, $|\nabla\phi|^2$ is such a term in the KS equation in the form used in [67][1]. Such a term also appears in the Kardar-Parisi-Zhang (KPZ) equation [64] and is also used in a nonvariational version of the SH equation [61]. One also finds μ_{nc}^{ng}-terms $(1-\tilde{\beta})\frac{v'(\phi)}{2}|\nabla\phi|^2 + (1+\beta)v(\phi)\Delta\phi$ with $v = \phi$ and $\beta = \tilde{\beta}$ in AC [5] and SH [72, 17] equations. Similar and higher order terms are used in Ref. [56]. Another option are dispersion terms proportional to $\partial_{xxx}\phi$ [18]. A related subtle way to break the gradient-dynamics structure is to combine conserved and nonconserved fluxes that individually have gradient-dynamics form as in (3) but correspond to different energy functionals $\mathscr{F}$. However, the difference can always be expressed as a particular form of μ_{nc}^{ng}. This occurs e.g. in some thin-film models with evaporation [9]. For further discussion of evaporation terms see [121].

The chapter is structured as follows. In section 2 we give a brief introduction to the general approach of numerical continuation for kinetic equations as (7) used in the framework of PDE2PATH and AUTO07P. Section 3 focuses on steady states

---

[1]Note that nongradient terms $|\nabla\phi|^2$ and $\phi\nabla\phi$ are often related by a transformation that, however, also transforms conserved into nonconserved dynamics, therefore here we explicitly list both expressions.

of the AC equation and the CH equation in 2d as well as on steady states of a variational form of the TF equation for partially wetting liquids on homogeneous and heterogeneous 2d substrates, while section 4 discusses the SH equation and a corresponding PFC model focusing on localized states in 1d and 2d. After the variational models selected nonvariational cases are treated. Section 5 considers the steady and time-periodic solutions of the KS equation in 1d, while §6 and §7 study a convective AC equation and a convective CH equation, respectively, in heterogeneous systems where pinning effects compete with lateral driving (again steady and time-periodic solutions in 1d). The final result section 8 focuses on a general nonvariational form of the TF equation studying stationary sliding drops in 2d and a transversal front instability in a dip-coating (or Landau-Levich) geometry. We summarize and give an outlook in the concluding section 9.

2 Continuation approach

We briefly review the (pseudo-)arclength continuation method to find solution branches and bifurcations for nonlinear equations depending on parameters. One important advantage over natural continuation is the ability to follow solution branches through saddle-node bifurcations, essential for many of the example systems analyzed in this chapter. The approach follows [65], see also [66]. Much of the theory can be formulated in general Banach spaces, but for simplicity we restrict ourselves to finite dimensions, and consider

$$M\frac{\mathrm{d}}{\mathrm{d}t}u = -G(u,\lambda), \tag{8}$$

where $u = (u_1,\ldots,u_{n_u}) \in \mathscr{X} = \mathbb{R}^{n_u}$ for instance denotes the nodal values of a spatial discretization of ϕ from (1). In the following we assume for notational simplicity that the matrix $M \in \mathbb{R}^{n_u \times n_u}$ is the identity, but it may also be singular; in the context of FEM discretizations as in PDE2PATH, it corresponds to the so-called mass matrix. Note that M plays no role for the computation of steady solutions of (8), but it influences the spectrum of the linearization $M\frac{\mathrm{d}}{\mathrm{d}t}v = -\partial_u G(u,\lambda)v$ around a steady solution. Further comments are given below. In the simplest case $G \in C^1(\mathscr{X} \times \mathbb{R}, \mathscr{X})$ and $\lambda \in \mathbb{R}$ stands for a scalar "active" parameter, but often (8) must be extended by n_q additional equations (constraints, or phase conditions), and to have one-dimensional continua of solutions we then need n_q additional active parameters. We explain some general ideas combined with some comments on how they are applied in AUTO07P and PDE2PATH.

2.1 Continuation of branches of steady solutions

For later generality, i.e., for adding constraints, in our notations we assume that $\lambda \in \mathbb{R}^{n_p}$, $n_p \geq 1$, is a parameter vector, but first let $n_p = 1$. We assume that $G \in C^1(\mathscr{X} \times \mathbb{R}, \mathscr{X})$ and consider an arc or "branch" $s \mapsto z(s) := (u(s), \lambda(s)) \in \mathscr{X} \times \mathbb{R}$ of steady solutions of (8), parametrized by $s \in \mathbb{R}$. We set up the extended system

$$H(u,\lambda) = \begin{pmatrix} G(u,\lambda) \\ p(u,\lambda,s) \end{pmatrix} = 0 \in \mathscr{X} \times \mathbb{R}, \tag{9}$$

where p is used to make s an approximation to arclength on the solution arc. The standard choice is as follows. Given s_0 and a point $(u_0, \lambda_0) := (u(s_0), \lambda(s_0))$, and

additionally a tangent vector $\tau_0 := (u_0', \lambda_0') := \frac{\mathrm{d}}{\mathrm{d}s}(u(s), \lambda(s))|_{s=s_0}$ we use, for s near s_0,

$$p(u, \lambda, s) := \xi \langle u_0', u(s) - u_0 \rangle + (1 - \xi) \langle \lambda_0', \lambda(s) - \lambda_0 \rangle - (s - s_0). \qquad (10)$$

Here $\langle u, v \rangle$ and $\langle \lambda, \mu \rangle$ are the inner products in $\mathbb{R}^{n_u}$ and $\mathbb{R}^{n_p}$, respectively, $0 < \xi < 1$ is a weight, and τ_0 is assumed to be normalized in the weighted norm

$$\|\tau\|_\xi := \sqrt{\langle \tau, \tau \rangle_\xi}, \qquad \left\langle \left(\begin{array}{c} u \\ \lambda \end{array} \right), \left(\begin{array}{c} v \\ \mu \end{array} \right) \right\rangle_\xi := \xi \langle u, v \rangle + (1 - \xi) \langle \lambda, \mu \rangle.$$

For fixed s, $p(u, \lambda, s) = 0$ thus defines a hyperplane perpendicular (in the inner product $\langle \cdot, \cdot \rangle_\xi$) to τ_0 at distance $\mathrm{d}s := s - s_0$ from (u_0, λ_0). A typical choice for ξ is $\xi = n_p/n_u$ which gives the parameter (vector) λ the same weight as the solution vector u in the arclength. We then use a predictor $(u^1, \lambda^1) = (u_0, \lambda_0) + \mathrm{d}s\, \tau_0$ for a solution (9) on that hyperplane, followed by a corrector using Newton's method in the form

$$\left(\begin{array}{c} u^{l+1} \\ \lambda^{l+1} \end{array} \right) = \left(\begin{array}{c} u^l \\ \lambda^l \end{array} \right) - \mathscr{A}(u^l, \lambda^l)^{-1} H(u^l, \lambda^l), \quad \text{where } \mathscr{A} = \left(\begin{array}{cc} G_u & G_\lambda \\ \xi u_0' & (1 - \xi)\lambda_0' \end{array} \right). \qquad (11)$$

Here $\mathscr{A}^{-1}H$ stands for the solution of the linear system $\mathscr{A}z = H$ by a suitable method, i.e., $\mathscr{A}^{-1}$ should never be computed, except maybe for small n_u. Since $\partial_s p = -1$, on a smooth solution arc we have

$$\mathscr{A}(s) \left(\begin{array}{c} u'(s) \\ \lambda'(s) \end{array} \right) = - \left(\begin{array}{c} 0 \\ \partial_s p \end{array} \right) = \left(\begin{array}{c} 0 \\ 1 \end{array} \right). \qquad (12)$$

Thus, after convergence of (11) yields a new point (u_1, λ_1) and Jacobian $\mathscr{A}$, the tangent direction τ_1 at (u_1, λ_1) with conserved orientation, i.e., $\mathrm{sign}\langle \tau_0, \tau_1 \rangle_\xi = 1$, can be computed from $\mathscr{A}\tau_1 = \left(\begin{array}{c} 0 \\ 1 \end{array} \right)$, with normalization $\|\tau_1\|_\xi = 1$. See Fig. 1 for a sketch.
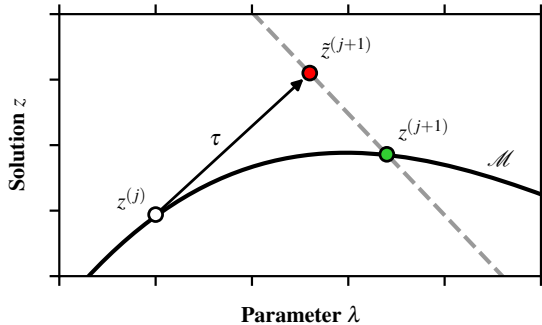

Figure 1: Sketch of pseudo-arclength continuation in the plane spanned by continuation parameter and solution measure.

The Jacobian $\mathscr{A}$ from (11) is nonsingular, except at steady bifurcation points (BPs), where two or more different branches of steady solutions intersect transversally. This follows from the so-called bordering lemma, see [57, Chapter 3]. In particular, at so-called regular fold points, where the branch turns around, G_u is singular but $\mathscr{A}$ is regular such that arclength continuation around fold points is no problem. Moreover, the predictor generically shoots beyond BPs, and the Newton method converges in cones around the branch with tips in the BPs, see, e.g., [66, §5.13].

2.2 Bifurcations

At BPs, eigenvalues $\mu(s)$ of G_u must cross the imaginary axis. These can either be real eigenvalues, which under mild additional assumptions yields a steady bifurcation, or a complex conjugate pair $\mu_\pm(s_0) = \pm i\omega(s_0)$ of eigenvalues, which under mild additional assumptions yields a Hopf bifurcation, i.e., the bifurcation of time periodic orbits ('Hopf orbits') for (8), with period near $2\pi/\omega(s_0)$ close to the bifurcation. To detect BPs, two simple methods which can also be used for large n_u, i.e., for (8) obtained from a spatial PDE discretization, are as follows. Here and in the following we always assume that we compare quantities evaluated at two points $z(s_1), z(s_2)$ on a branch, at distance ds. Of course, all algorithms must fail if, e.g., a simple eigenvalue of $G_u(u(s))$ or $\mathscr{A}(s)$ moves back and forth between s_1 and s_2, e.g., if the step size ds is too large.

(a) Monitor sign changes of det$\mathscr{A}$. This is cheap if a lower upper (LU) decomposition of $\mathscr{A}$ is available, which is usually the case if direct solvers are used for the linear systems in (11). On the other hand, sign changes of det$\mathscr{A}$ only detect an odd number of eigenvalues crossing, and in particular cannot detect Hopf bifurcations.

(b) Compute (by, e.g., inverse vector iteration) a (small) number of eigenvalues μ of G_u closest to 0 (and possibly also closest to spectral shifts $i\omega_j$, $\omega_j \in \mathbb{R}$), and monitor the number of these eigenvalues with real parts greater than zero. This works well for dissipative problems where only few eigenvalues are close to the imaginary axis, and where, to detect Hopf bifurcations, guesses for suitable ω_j are available. A method to obtain such guesses, and ways in which the algorithm may fail, are explained in [132, §2.1].

After *detection* of a BP (or rather a possible BP, due to possibly spurious detection of BPs using method (b)), the BP should be *localized*, i.e., its position between $z(s_0)$ and $z(s_1)$ should be computed. A simple way to do this is bisection, based on either (a) or (b) as in the original detection.

Various other methods for detection and localization of BPs have been suggested and implemented. Some of these are only suitable for small n_u, for instance computing *all* eigenvalues of $\mathscr{A}$, or using bialternate products [75, §10.2.2]. Other methods use so called minimally extended systems, in particular, for localization, where typically the dimension of the problem is doubled or tripled. Again see [75, Chapter 10], or for instance [84, Chapter 3].

After localization of a BP we want to compute 'the other' branches which bifurcate from the branch we continued so far. This branch switching is again a predictor-corrector method, and for steady bifurcations the main task is to compute tangents to the bifurcating branches. We call a BP a *simple bifurcation point* if exactly one simple eigenvalue goes through zero, such that exactly two (steady)

branches intersect at this point. For simple BPs, branch switching is easy, i.e., the bifurcation direction follows from explicit formulas, see e.g., [65]. Similarly, for (simple, i.e., exactly one bifurcating Hopf branch) Hopf bifurcations there are somewhat more lengthy formulas to obtain approximations of solutions on the bifurcating branches, see, e.g., [75, p531-536]. To proceed similarly for multiple BPs, we need to find isolated solutions of the pertinent 'algebraic bifurcation equations'. This may be a difficult problem if it is not clear a priori that the bifurcating branches are determined at some reasonably low order k. See, e.g., [84, §6.4] for further discussion of this determinacy problem, and a general algorithm. However, to the best of our knowledge this has not been implemented in full generality in any package, and has only recently been partially implemented in PDE2PATH [133]. For multiple Hopf bifurcations, the situation quickly becomes very complicated, see, e.g., [75, Chapter 10], but for instance MATCONT can deal with a large number of cases (in the low dimensional setting).

2.3 Continuous symmetries and phase conditions

If (1) has continuous symmetries, for instance a boost invariance or translational invariance, such that even for fixed primary parameter λ there is a nontrivial continuous family $\sigma \mapsto \phi(\cdot, \lambda, \sigma)$ of solutions, then the linearization around ϕ is always singular. For instance, for a translational invariant (1d) problem $\partial_t \phi = F(\phi)$, if $F(\phi(\cdot)) = 0$, then $F(\phi(\cdot + \sigma)) = 0$ for all $\sigma \in \mathbb{R}$, hence $0 = \frac{d}{d\sigma} F(\phi(\cdot + \sigma))|_{\sigma=0} = \partial_\phi F(\phi) \partial_x \phi$ such that $\partial_x \phi$ is in the kernel of $\partial_\phi F(\phi)$.

Such symmetries are approximately inherited by the discretized problem (8). Thus, $\mathscr{A}$ from (11) is almost singular, and the neutral directions must be removed by appropriate phase conditions, for which we use the general notation

$$Q(u, \lambda) = 0 \in \mathbb{R}^{n_q}, \tag{13}$$

where now $\lambda = (\lambda_{\text{org}}, \lambda_{\text{add}}) \in \mathbb{R}^{n_p} = \mathbb{R}^{1+n_q}$, where $\lambda_{\text{add}} \in \mathbb{R}^{n_q}$ stands for the required additional parameters. For PDEs, the two most common examples are mass conservation

$$q_1(u, \lambda) = \frac{1}{|\Omega|} \int_\Omega u \, d\mathbf{r} - m_0 = 0, \tag{14}$$

where m_0 is a reference mass, and phase conservation (here written for the case of translational invariance in x)

$$q_2(u, \lambda) = \int_\Omega u \partial_x u^* \, d\mathbf{r} = 0, \tag{15}$$

where u^* is a reference profile, and expressions such as $\int u \, d\mathbf{r}$ and $\partial_x u^*$ are understood as the discrete analogs of the respective expressions for ϕ. The associated additional parameters λ_{mass} for q_1 and λ_{phase} for q_2 are then introduced into (8) in the form $\partial_t u = -G(u, \lambda) + \lambda_{\text{mass}}$ and $\partial_t u = -G(u, \lambda) + \lambda_{\text{phase}} \partial_x u$, respectively, where the latter corresponds to a transformation to a comoving frame with speed λ_{phase}. AUTO07P and PDE2PATH have general interfaces to add (13) to the original problem (8). In detail, by augmenting u with the suitable parameters and setting the appropriate lines of M in (8) to zero, Q can be appended to G in (8), and this is done internally, exploiting the flexibility obtained from M.

Examples for mass conservation, phase conservation and a combination of both are given in sec. 4, 5 and 8, respectively. The conservation of mass (14) in sec. 5,

for example, is achieved by adding a fictitious flux ε to the time evolution, i.e., $\partial_t \phi = \ldots + \varepsilon$. This additional free parameter is then automatically kept at zero during continuation with side condition (14).

2.4 Hopf bifurcation and time periodic orbits

To compute and continue Hopf orbits, i.e., time-periodic orbits with periods near $2\pi/\omega_0$ close to the bifurcation, a standard method is to rescale time $t \rightarrow t/T$ with an unknown parameter T, $T = 2\pi/\omega_0$ at bifurcation, and consider

$$M\frac{\mathrm{d}}{\mathrm{d}t}u = -TG(u,\lambda), \quad u(0) = u(1). \tag{16}$$

Since (16) is autonomous, and hence any translation of a solution $t \mapsto u(t)$ is again a solution, we need a phase condition, for instance

$$q := \int_0^1 \langle u(t), \dot{u}_0(t) \rangle \, \mathrm{d}t, \tag{17}$$

and the step length p from (9) changes to, e.g.,

$$p := \xi_{\mathrm{H}} \int_0^1 \langle u(t) - u_0(t), u_0'(t) \rangle \, \mathrm{d}t + (1 - \xi_{\mathrm{H}}) \big[w_T (T - T_0) T_0' + (1 - w_T)(\lambda - \lambda_0)\lambda_0' \big], \tag{18}$$

where again u_0, T_0, λ_0 are from the previous step, ξ_{H} and w_T denote weights for the u and T components of the unknown solution, and the integrals in (18) (and in (17)) are discretized based on a time discretization $t_0 = 0 < t_1 < \ldots < t_m = 1$. For a piecewise linear discretization (in t), the full unknown discrete solution u then is a vector in $\mathbb{R}^{mn_u}$. Setting $z = (u, T, \lambda)$ and writing (16) as $\mathscr{G}(z) = 0$ we thus obtain the extended system

$$H(U) := \begin{pmatrix} \mathscr{G}(z) \\ q(u) \\ p(z) \end{pmatrix} \overset{!}{=} \begin{pmatrix} 0 \\ 0 \\ 0 \end{pmatrix} \in \mathbb{R}^{mn_u+2}. \tag{19}$$

The (in)stability of and possible bifurcations from a periodic orbit u are analyzed via its Floquet multipliers γ, which are obtained from finding nontrivial solutions (v, γ) of the variational boundary value problem

$$M\frac{\mathrm{d}}{\mathrm{d}t}v(t) = -T\partial_u G(u(t))v(t), \quad v(1) = \gamma v(0). \tag{20}$$

By translational invariance of (16), there is always the trivial multiplier $\gamma_1 = 1$, and u_H is (orbitally) stable if all other multipliers have modulus less than 1. Moreover, a necessary condition for the bifurcation from a branch $\lambda \mapsto u_H(\cdot, \lambda)$ of periodic orbits is that at some $(u_H(\cdot, \lambda_0), \lambda_0)$, additional to the trivial multiplier $\gamma_1 = 1$ there is a second multiplier γ_2 (or a complex conjugate pair $\gamma_{2,3}$) with $|\gamma_2| = 1$, see, e.g., [108, Chapter 7] or [75]. For certain types of t discretizations, the Floquet multipliers can be obtained from the Jacobian $\partial_u \mathscr{G}(u_H)$ [79], see also [132, §2.4], but for large scale problems this becomes expensive, and in general the computation of Floquet multipliers is a difficult problem.

If the original PDE has continuous symmetries and thus the computation of steady (or traveling wave) solutions requires n_q phase conditions (13), then the

computation of Hopf orbits requires suitable modifications of these phase conditions. This is in general not straightforward since (13) is not of the form $\partial_t u = Q(u, \lambda)$ and thus cannot simply be appended to (8), if the time steppers or boundary value problem (in t) solvers cannot deal with singular M in (8), or (16). In §5 we proceed by example and consider the Kuramoto-Sivashinsky equation with periodic boundary conditions. For the computation of steady branches and branches of traveling waves, this requires two phase conditions of type (14) and (15), and in §5 we explain how to modify these for the computation of Hopf orbits, i.e., for standing waves and modulated traveling waves.

2.5 Some packages

The above ideas are the basis for a number of numerical continuation and bifurcation packages, with different foci and emphasis. Two highly developed and established packages are AUTO07P [35] and MATCONT [32]. Both are originally aimed at genuine ODEs, i.e., low-dimensional algebraic problems for the case of steady solutions, and are very powerful for this setting. Both have also been applied to PDE problems after spatial discretization, but this becomes problematic for large n_u, mostly because the numerical linear algebra is aimed at ODEs.

The rather recent package PDE2PATH [135, 131] is specifically aimed at PDEs. In particular, it provides convenient user interfaces to obtain the form (8) for a rather large class of PDE problems in 1d, 2d, and 3d. Mesh and FEM space generation, including adaptive mesh refinement, work rather automatically, and the application of PDE2PATH to model problems of various types with various boundary conditions is explained in a number of demo directories and tutorials, available at [131]. On the other hand, PDE2PATH is as yet restricted to steady bifurcations, Hopf bifurcations, periodic orbits and their Floquet multipliers (up to medium size problems) and a few codimension-2 problems, but does not yet deal with, e.g., secondary bifurcations from Hopf orbits, and thus does not yet provide the same completeness and generality for PDEs that AUTO07P and MATCONT provide for genuine ODE problems.

Other software used for large scale problems include CL_MATCONT [33], which has a focus on invariant subspace continuation that makes it suitable for larger scale computations [11], or COCO [30] which is a general toolbox and for instance in [48] has been coupled with COMSOL for a PDE problem. See also LOCA [103] or OOMPHLIB [59] for continuation and bifurcation tools (libraries) aimed at PDEs. Concerning the continuation of periodic orbits, the collocation method used in PDE2PATH may not be efficient for large scale problems, i.e., for more than 30.000 DoF in space, combined with more than 20 DoF in time. For such problems, shooting methods appear to be more appropriate, see, e.g., [104] for impressive results. On the other hand, these and many other continuation/bifurcation results for PDEs in the literature, see also [34, 90] for reviews, seem to be based on custom made codes, which sometimes do not seem easy to access and to modify for nonexpert users, although [105] provides an excellent review of recipes for continuation based on time steppers and shooting methods.

In this contribution we aim to portray what can be done for problems of type (1) with AUTO07P and PDE2PATH. Implementation details for the PDE2PATH examples can be found in the appendix of [45] and the tutorials at [131], which in particular illustrate that all the examples can be treated in a convenient unified way, which require only a few user-provided MATLAB functions.

3 Steady states of Allen-Cahn- and Cahn-Hilliard-type equations

3.1 Model

The first and most simple examples we are examining are the Allen-Cahn (AC) equation and the Cahn-Hilliard (CH) equation. The AC equation is obtained by neglecting mass-conserving and nongradient contributions in Eq. (7) and by introducing a constant mobility in the nonmass-conserving flux:

$$Q_c = \mathbf{j}_c^{ng} = \mu_{nc}^{ng} = 0 \quad \text{and} \quad Q_{nc} = 1\,. \tag{21}$$

The CH equation is obtained by neglecting nonmass-conserving and nongradient contributions in Eq. (7) and introducing a constant mobility in the mass-conserving flux:

$$\mu_c^{ng} = \mathbf{j}_c^{ng} = Q_{nc} = \mu_{nc}^{ng} = 0 \quad \text{and} \quad Q_c = 1\,. \tag{22}$$

The energy functional

$$\mathscr{F}[\phi] = \int_\Omega \frac{\sigma}{2}\,(\nabla\phi)^2 + f(\phi) - \mu\phi\,\mathrm{d}\mathbf{r}\,. \tag{23}$$

is based on Eq. (5) and consists of the sum of an interfacial term $\sim (\nabla\phi)^2$, a bulk energy $f(\phi)$ and an additional term $-\mu\phi$ where μ corresponds to an external field or chemical potential. The bulk energy can have different forms, here, a simple double well potential

$$f(\phi) = -\frac{1}{2}\phi^2 + \frac{1}{4}\phi^4 \tag{24}$$

is employed. An example for a more complicated potential is described is §8. Determining on the one hand the flux j_{nc}^g in the AC case by variation of the functional (23), the governing equation (7) becomes a second order PDE that is the evolution equation of the nonconserved concentration field $\phi(\mathbf{r},t)$

$$\partial_t\phi = \sigma\Delta\phi + \phi - \phi^3 + \mu\,, \tag{25}$$

i.e., the well-known Allen-Cahn equation. Determining on the other hand the flux $\mathbf{j}_c^g$ in the CH case with the energy functional (23) leads to the fourth order PDE that is the evolution equation of the conserved concentration field $\phi(\mathbf{r},t)$

$$\partial_t\phi = -\Delta\left[\sigma\Delta\phi + \phi - \phi^3\right] \tag{26}$$

that is often investigated in the context of phase separation of a binary mixture [21, 76, 41] with discussions of, e.g., solutions on 1d and 2d domains in Refs. [92, 93, 125] and Refs. [81, 80, 15], respectively.

To examine the steady states of eqs. (25) and (26) one sets $\partial_t\phi = 0$ and obtains

$$0 \quad = \quad \sigma\Delta\phi + \phi - \phi^3 + \mu \tag{27}$$

$$\text{and} \quad 0 \quad = \quad -\Delta\left[\sigma\Delta\phi + \phi - \phi^3\right]\,, \tag{28}$$

respectively. Further, eq. (28) can easily be transformed into eq. (27) by performing two spatial integrations. Thereby the first integration constant is zero for no-flux boundaries and the second integration constant is denoted μ. Importantly,

for eq. (27) as steady AC equation, μ is the imposed external field or chemical potential, but for eq. (27) as steady CH equation, μ takes the role of a Lagrange multiplier for mass conservation. This implies that μ is directly (but nonlinearly) related to the mean concentration

$$\phi_0 = \frac{1}{\Omega} \int_\Omega \phi \, d\mathbf{r}. \tag{29}$$

The different meaning of μ for the steady AC and CH cases implies that different types of bifurcation curves can be calculated in the two cases and stabilities of the same solutions may differ in the AC and CH context.

3.2 Continuation

As eq. (27) is a second order semilinear equation the implementation in PDE2PATH is straightforward as described in the tutorials given in the appendix of [45]. Here, we use a square with side lengths $l_x = l_y = 32\pi$ with Neumann boundary conditions. As the latter explicitly break the translational symmetry and the mean concentration is not imposed but adjusts with μ as external parameter, no integral side conditions are needed and there is only one continuation parameter in each continuation run.
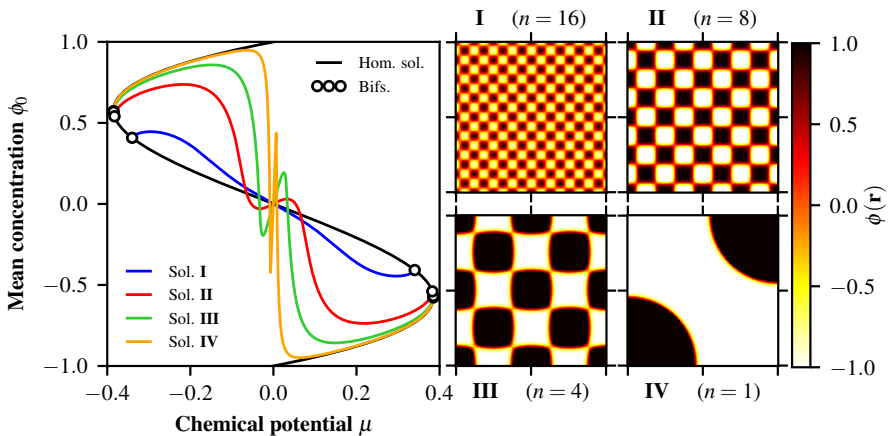

Figure 2: (left) Branches of homogeneous and inhomogeneous steady state solutions of the Allen-Cahn equation (27) on a square domain ($l_x = l_y = 32\pi$) with Neumann BC. Shown is the mean concentration ϕ_0 in dependence of the chemical potential μ. (right) Selected solution profiles for $\sigma = 1.0$ $\mu = 0.1$, $\phi_0 \neq 0$ and different wave numbers $k_x = k_y = n/(16\sqrt{2})$ with $n \in \{1, 4, 8, 16\}$.

We use μ as continuation parameter, while the mean concentration ϕ_0 is calculated as solution measure. The obtained bifurcation diagram is shown in fig. 2. As starting solution we employ the trivial steady state solution $\phi = \phi_0 = -1$ at $\mu = 0$ and fix the interfacial stiffness to $\sigma = 1$. The first obtained branch (black line in fig. 2) consists of homogeneous solutions that are analytically known and

12

characterized by

$$0 = \phi_0 - \phi_0^3 + \mu.$$ (30)

The branch has two saddle-node bifurcations at $(\mu, \phi_0) = \pm(2/3\sqrt{3}, -1/\sqrt{3})$. On the sub-branch that connects the saddle-node bifurcations one detects various primary pitchfork bifurcations where inhomogeneous steady states of different wave numbers emerge. The wave numbers $\mathbf{k} = (k_x, k_y)^T$ with $k_x = k_y = n/(16\sqrt{2})$ are selected by the employed Neumann BC. These inhomogeneous solutions correspond to phase-separated states where $\phi = \pm 1$ represent the two phases. Note that here we only show as an example a particular pattern type, namely, square patterns with $\mathbf{k}$ oriented along the diagonal. One-dimensional patterns, i.e., stripe patterns, and square patterns with wave vectors parallel to the boundaries do also exist on square domains.

We end this section with a remark on the different interpretation of fig. 2 as bifurcation diagram either for the AC or for the CH equation. In the former case, μ is the control parameter and ϕ_0 is the solution measure. Then the bifurcation diagram fig. 2 indicates that along the individual branches of heterogeneous solutions stabilities do not change (i.e., no eigenvalue crosses zero) as there are no saddle-node bifurcations on these branches (and we neglect the possibility of symmetry changing bifurcations). However, in the latter case we have to flip the diagram: now the mean concentration ϕ_0 is the control parameter and μ acts as corresponding Lagrange multiplier and in a sense may be considered a solution measure. Looking at fig. 2 in this way (turning the page $90°$ to the left) shows that then saddle-nodes occur also on the branches of heterogeneous solutions, i.e., stabilities change along the branches. In other words, the same states may show different stabilities depending on the allowed dynamics - mass-conserving in the CH case and nonmass-conserving in the AC case - as the different dynamics allow for different classes of perturbations.

3.3 Variational thin-film equation

Another Cahn-Hilliard-type equation is the thin-film equation of mesoscopic hydrodynamics that describes films and drops of nonvolatile, partially wetting liquid on homogeneous or heterogeneous horizontal substrates [94, 86, 119, 12, 120]. The conserved field $\phi(\mathbf{r}, t)$ then corresponds to the local film height.[2] It is obtained from Eq. (7) by neglecting nonmass-conserving and nongradient contributions and introducing a cubic mobility in the mass-conserving flux:

$$\mu_c^{ng} = \mathbf{j}_c^{ng} = Q_{nc} = \mu_{nc}^{ng} = 0 \quad \text{and} \quad Q_c = \frac{\phi^3}{3}.$$ (31)

The energy functional is eq. (5) where σ now corresponds to the liquid-gas interface tension and the local energy $f(\phi)$ becomes the wetting potential

$$f(\phi, \mathbf{r}) = (1 + \xi g(\mathbf{r})) \left[-\frac{1}{2}\phi^{-2} + \frac{1}{5}\phi^{-5} \right]$$ (32)

which here explicitly depends on the spatial coordinates via a heterogeneity function $g(\mathbf{r})$ encoding $O(1)$ variations and the wettability contrast ξ. This models

---

[2]Note that for ultrathin films it can be related to the adsorption per substrate area. This makes it possible to consider transitions between convective dynamics of the bulk of a drop and diffusive dynamics of a molecular adsorption layer (or precursor film) covering the substrate outside the drop [141].

spatial variations of the wettability of the substrate. This particular wetting potential combines two antagonistic power laws [86, 97] and allows for the coexistence of a macroscopic drop of equilibrium contact angle $\theta_e = \sqrt{-2f(\phi_a)/\sigma} = \sqrt{3(1+\xi g)/5\sigma}$ with an adsorption layer of height $\phi_a = 1$ that represents a "moist" substrate.[3] The resulting thin-film evolution equation is

$$\partial_t \phi = -\nabla \cdot \left[\frac{\phi^3}{3} \nabla \left(\sigma \Delta \phi + (1 + \xi g(\mathbf{r})) \left[-\phi^{-3} + \phi^{-6} \right] \right) \right]. \tag{33}$$

In §8 a more general form the thin-film equation with nonvariational terms is analyzed.

To investigate steady states, we set $\partial_t \phi = 0$ and integrate twice to obtain

$$0 = -\sigma \Delta \phi - (1 + \xi g(\mathbf{r})) \left[-\phi^{-3} + \phi^{-6} \right] - p. \tag{34}$$

after nondimensionalization. Here, the integration constant p has the physical dimension of a pressure and in the present mass-conserving CH-type case acts as Lagrange multiplier for mass conservation. Note that in a nonmass-conserving AC-type case it would be an externally imposed vapor pressure.

With the exception of the explicit spatial dependence of $f(\phi, \mathbf{r})$, the implementation and boundary conditions are equivalent to the ones used in §3.2. By extending the numerical domain $\Omega = [-l_x/2, l_x/2] \times [-l_y/2, l_y/2]$ with Neumann boundaries to a physical domain $\Omega_e = [-l_x, l_x] \times [-l_y, l_y]$ with periodic boundaries in the case of a homogeneous substrate (i.e., for $\xi = 0$) we determine the bifurcation diagram in fig. 3 using the mean film height ϕ_0 as control parameter and the energy $\mathcal{F}$ relative to the energy of a flat film of identical ϕ_0 as solution measure

$$\mathcal{F}_{\text{rel}}[\phi] = \mathcal{F}[\phi] - \mathcal{F}[\phi_0] = \mathcal{F}[\phi] - \Omega f(\phi_0). \tag{35}$$

Note, however, that p acts as Lagrange multiplier that has to be adapted as second continuation parameter because mass is controlled via an integral side condition (29).

The continuation is started with a trivial flat film solution with $\phi = \phi_0 = 1$. Continuing in ϕ_0 (and adapting p) the first run follows the branch of homogeneous films (horizontal line in fig. 3 detecting various pitchfork bifurcations that weakly nonlinear theory identifies as subcritical bifurcations (not shown here, see [45, chapter 3]). Again, at the pitchfork bifurcations various nontrivial branches of patterned states of different wave numbers emerge. Here, we focus on branches of solutions with one or two drops (D1 and D2) and with one or two ridges (R1 and R2). As D1 and R1 have the same wave number $k = 1/24$, these patterns bifurcate at the same bifurcations. Furthermore, these drop and ridge branches of solutions of identical wave number are connected by secondary branches emerging from the primary branches at secondary pitchfork bifurcations that break respective symmetries. A linear stability analysis of the flat film shows its instability for $1.26 < \phi_0 < 6.45$ where spinodal dewetting is expected [118]. However, the linearly stable flat film solutions for $6.45 < \phi_0 < 12.43$ coexist with drop and ridge solutions of lower free energy and are therefore metastable. Perturbations of specific forms and amplitude above a certain threshold (related to the threshold solutions on the subcritical part of the respective branches) may still trigger dewetting

---

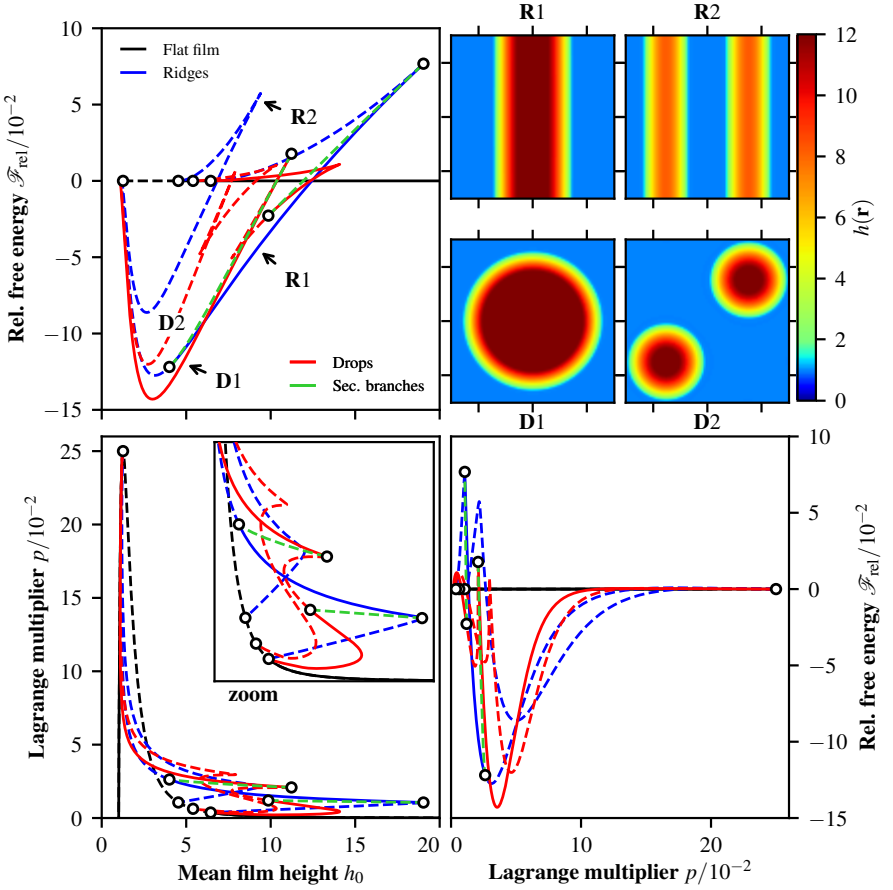[3]Consider the discussion of dry and moist case in Ref. [53].

Figure 3: Steady state solutions of the thin-film equation for partially wetting liquids on a homogeneous substrate, i.e., solutions of eq. (34) with $\sigma = 1.0$, $\xi = 0$. The top left panel shows the bifurcation diagram in terms of the energy $\mathscr{F}_{\text{rel}}$ relative to the energy of a flat film in dependence of the mean film height ϕ_0 while the bottom left panel gives the corresponding Lagrange multiplier p. Linearly stable and unstable solutions (bzgl. CH-type dynamics) are indicated by solid and dashed lines, respectively. The top right panel shows selected corresponding solution profiles on a domain $\Omega_{\text{e}} = [-l_x, l_x] \times [-l_y, l_y]$ with periodic boundary conditions with $l_x = l_y = 24\pi$. Finally, the bottom right panel gives the energy $\mathscr{F}_{\text{rel}}$ in dependence of the pressure p (note that stability is also in this panel indicated for the CH-type dynamics, not the AC-type dynamics).

processes. Depending on the mean film height, the globally stable profiles of minimal free energy are given either by the one-drop (**D**1) or one-ridge (**D**1) solution. The transition between them is related to the Plateau-Rayleigh instability of liquid ridges. Figure 3 shows that it is hysteretic and involves metastable regions where finite perturbations are needed to transform ridges into drops or vice versa. Patterns of larger wave numbers, e.g., the solutions **D**2 and **R**2 are always linearly unstable w.r.t. coarsening modes.

As in section 3.2 we briefly discuss the consequences of the different roles the parameter p takes (i) on the one hand in the context of a mass-conserving CH-type dynamics as the thin-film equation (33) and (ii) on the other hand in the context of a nonmass-conserving AC-type dynamics on the same energy functional. In the former case (i), p is the Lagrange multiplier that is adapted during the continuation run. It depends in a nonlinear manner on ϕ_0 as shown in the lower left panel of fig. 3. At pitchfork and saddle-node bifurcations in the left panels of fig. 3 the stabilities of the various solutions with respect to mass-conserving perturbations change. However in the latter case (ii) of a nonmass-conserving dynamics (condensation/evaporation), other perturbations are allowed and therefore the stabilities change. In this case, p controls the behavior as external field and ϕ_0 adapts, i.e., the bottom left panel of fig. 3 can be used as bifurcation diagram if looked at from the left. The bottom right panel gives the corresponding bifurcation diagram showing the energy $\mathscr{F}$ in dependence of the imposed p. Again, as in section 3.2, this change in perspective results in different stability properties of the same solutions, indicated by the absence of saddle-node bifurcations in the bottom right panel of fig. 3.

However, the stability properties of the solutions and the bifurcation structure in the upper left panel of fig. 3 may also change when the wettability of the substrate is modulated [124] in the case of the mass-conserving dynamics (33). Employing, for instance, a stripelike heterogeneity function

$$g(\mathbf{r}) = -\cos\left(\pi N x/2l_x + \pi(N-1)\right) \tag{36}$$

that models a substrate with N hydrophilic stripes, it is possible to stabilize a solution of N ridges against coarsening. In the $N = 2$ case corresponding to the **R**2 solutions observed on the homogeneous substrate, we use a wettability contrast $\xi = 1.0$ and generate the bifurcation diagram shown in fig. 4. For the heterogeneous system, the flat film solution does not exist any more but is replaced by a solution of type **R**2. In the parameter range $1.0 < \phi_0 < 2.74$ this solution is now linearly stable. For larger mean film heights, solution profiles with one ridge parallel (**R**1) or perpendicular (**R**1$^+$) to the wettability pattern are linearly stable and/or of minimal energy. The system is analyzed in more detail in [45].

4 Steady states of Swift-Hohenberg equation and Phase-Field-Crystal model

4.1 Model

Another important example of pattern forming models with a scalar order parameter field is the Swift-Hohenberg (SH) equation [117, 28]. It is obtained from Eq. (7) by neglecting mass-conserving and nongradient contributions, introducing
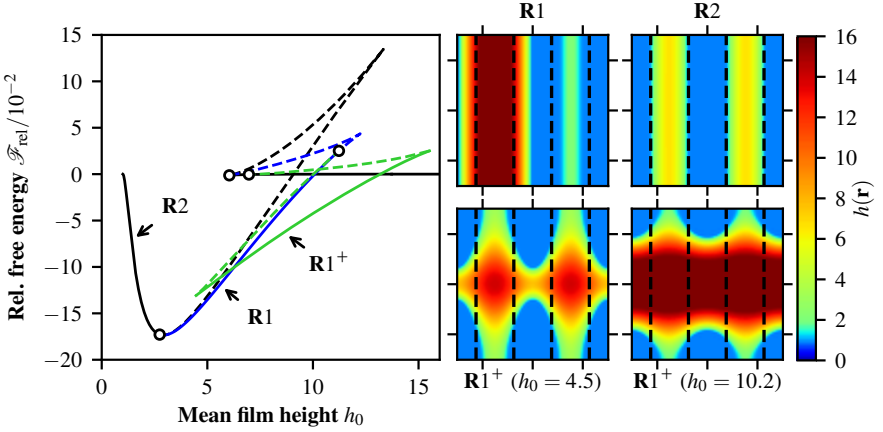
Figure 4: Steady state solutions of the thin-film equation for partially wetting liquids on a heterogeneous substrate with two hydrophilic stripes, i.e., solutions of eqs. (34) and (36) with $\sigma = 1.0$, $\xi = 1.0$ and $N = 2$. The left panel shows the bifurcation diagram in dependence of the mean film height ϕ_0 employing again the energy $\mathscr{F}_{\mathrm{rel}}$ relative to a flat film solution which, however, is no longer a steady state of the given heterogeneous system. Linearly stable and unstable solutions are indicated by solid and dashed lines, respectively. The right panel shows selected corresponding solution profiles for a domain as in fig. 3.

a constant mobility in the nonmass-conserving flux, i.e.,

$$Q_c = \mathbf{j}_c^{ng} = \mu_{nc}^{ng} = 0 \quad \text{and} \quad Q_{nc} = 1, \tag{37}$$

and employing the energy functional (6) with $\kappa = \sigma = 1$ and

$$f(\phi) = \frac{1}{2}(1+r)\phi^2 - \frac{\delta}{3}\phi^3 + \frac{1}{4}\phi^4 \tag{38}$$

This particular SH equation (also other f are common) reads[4]

$$\partial_t \phi = -(1+\Delta)^2 \phi - r\phi + \delta\phi^2 - \phi^3. \tag{39}$$

In contrast, the Phase-Field-Crystal (PFC) model [44], aka conserved Swift-Hohenberg (cSH) equation [123], is obtained by neglecting nonmass-conserving and nongradient contributions in Eq. (7) and introducing a constant mobility in the mass-conserving flux, i.e.,

$$\mu_c^{ng} = \mathbf{j}_c^{ng} = Q_{nc} = \mu_{nc}^{ng} = 0 \quad \text{and} \quad Q_c = 1. \tag{40}$$

It reads

$$\partial_t \phi = \Delta \left[(1+\Delta)^2 \phi + r\phi - \delta\phi^2 + \phi^3 \right]. \tag{41}$$

The corresponding stationary equation is as in §3 derived by setting $\partial_t \phi = 0$ in eq.(41) and integrating twice, obtaining

$$0 = \Delta^2 \phi + 2\Delta\phi + (1+r)\phi - \delta\phi^2 + \phi^3 - \mu + \varepsilon_1 \partial_x \phi + \varepsilon_2 \partial_y \phi. \tag{42}$$

where again μ represents the Lagrange multiplier for mass conservation. However, eq. (42) also describes steady states of the SH equation (39). In this case μ represents an imposed external field or chemical potential and is in most works implicitly set to zero. To break the translational invariances in x- and y-direction in the case of periodic boundary conditions we implement two respective phase conditions as described in §2.3. These imply that two additional continuation parameters are needed. We chose the fictitious advection speeds $\varepsilon_{1,2}$ (see comoving frame terms in eq. (42)).

The standard stationary SH equation corresponds to eq. (42) with $\delta = \mu = 0$ [28]. Employing r as control parameter, its trivial state $\phi = 0$ becomes unstable at a supercritical pitchfork bifurcation where a branch of stable steady spatially periodic states emerges. As there is no Maxwell point where linearly stable trivial and periodic states coexist, the system shows no localized solutions. However, such a Maxwell point exists when choosing either $\delta \neq 0$ [19] or $\mu \neq 0$ [123] and one can discuss the occurrence of aligned or slanted homoclinic snaking of localized states.

4.2   Continuation

In contrast to the steady AC/CH equation (27), the steady SH/PFC equation (42) is a fourth order semilinear PDE. To implement this equation in PDE2PATH we have two options: (i) One may split the fourth order equation into a system of two second order equations by defining a second scalar field $u = \Delta\phi$ (see eqs. (44) and

---

[4]Note that different sign conventions for r are in use.

(45) below). (ii) The fourth order right hand side can be implemented directly by restricting the system to periodic boundary conditions. Here, we follow the second option that includes the periodic boundary conditions. To break the resulting translational invariance of the system we employ a phase condition analogue to eq. (15), i.e., adding another continuation parameter beside the principal one. As solution measure we use the norm

$$||\delta\phi|| := \frac{1}{\Omega} \int_{\Omega} |\phi - \phi_0| \, d\mathbf{r}. \tag{43}$$
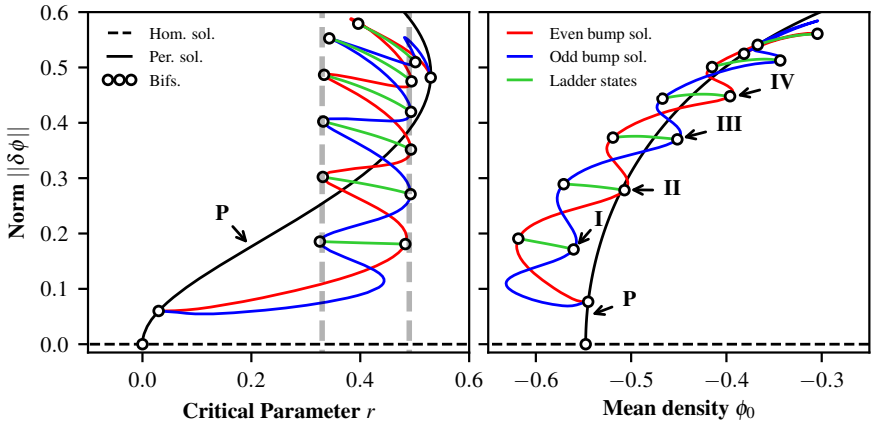
Figure 5: (left) Aligned and (right) slanted homoclinic snaking branches of localized state of the one-dimensional steady Swift-Hohenberg equation (42) for (left) $\delta = 2$, $\mu = 0$ and (right) $\delta = 0$, $r = -0.9$, $\mu \neq 0$, respectively.

As starting point we again use a trivial homogeneous solution and obtain bifurcation diagrams as in fig. 5 employing, e.g., the parameter r or the mean density ϕ_0 as control parameter. As first example we look at the (nonmass-conserving) SH equation with $\delta = 2$ and $\mu = 0$ in 1d, and continue the homogeneous solution branch in the parameter r, detect the primary bifurcations where the branch of periodic solutions (**P**) emerges. Following the branch of periodic states we detect secondary bifurcations where two branches of localized states bifurcate, namely, of reflection-symmetric states with even and odd number of "bumps", respectively. Typical solution profiles are shown in fig. 6. The second continuation parameter is given by the fictitious advection speed ε_1 which is kept at zero by simultaneously fulfilling the phase condition as given in eq. (15). The branches of localized states snake upwards in an intertwined manner, adding a pair of bumps per pair of saddle-node bifurcations and finally terminate again on the branch **P** when the localized structure fills the available space. The "snake and ladder" structure is completed by "runge" branches of asymmetric localized solutions that emerge at tertiary bifurcations and connect the two branches of symmetric localized solutions. For more details on this see, e.g., refs. [19, 20]. Note that the left- and right-hand saddle-node bifurcations are at respective identical values of the control parameter marked in fig. 5(left) by vertical dashed gray lines. This is called aligned snaking.
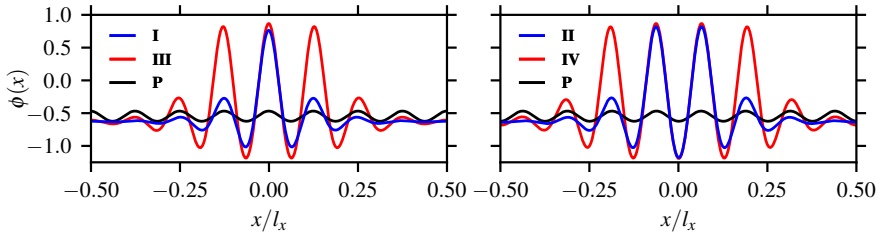
19

Figure 6: Profiles of one-dimensional localized states of (42) calculated for $\delta = 0$, $r = -0.9$ and $\mu \neq 0$ corresponding to the branches shown in fig. 5(right). The left panel shows states with an odd number of bumps whereas the right panel shows solutions of an even number of bumps.

In contrast, fig. 5(right) shows slanted (or tilted) snaking where the subsequent respective left and right saddle-node bifurcations are not vertically aligned. This is, e.g., typical for snaking branches of localized solutions for systems that involve a conservation law [14, 31, 123]. Here, we solve equation (42) with $\delta = 0$ and use the mean density ϕ_0 as primary continuation parameter, ε as further continuation parameter (translation invariance) and also have to add the Lagrange multiplier μ as the third one (as mass conservation gives another integral side condition). The topology of the bifurcation diagram and sequence of branches is the same as in fig. 5(left). Solution profiles are given in fig. 6. Note that the linear stability of solutions is not shown here, cf. Remark 1 at the end of this section. In general, the localized states switch from linearly stable to unstable at the saddle node bifurcations whilst all the ladder states are unstable. The remark in §3 on the dependence of the stability of solutions on the character of the considered dynamics also applies here.

For a two dimensional domain, we can obtain similar solution branches as shown for a hexagonal domain in fig. 7 in the mass-conserving case, i.e., using mean density ϕ_0 as principal continuation parameter. To increase computational efficiency we make use of the spatial symmetries and instead of the full hexagonal domain only use one of twelve equivalent triangles defined by the vertices $(x, y) = 4\pi(0,0)$, $4\pi(0, 4/\sqrt{3})$ and $4\pi(1, \sqrt{3})$ employing Neumann boundary conditions. Therefore we use option (i) introduced above and split the stationary equation (42) into the two second order equations

$$0 = \Delta\phi - u \tag{44}$$
$$\text{and} \quad 0 = \Delta u + 2u + (1+r)\phi - \delta\phi^2 + \phi^3 - \mu. \tag{45}$$

The first equation (44) defines a second field u as the laplacian of ϕ and the second equation (45) is the steady SH equation written using both fields.

The continuation in ϕ_0 (adapting the Lagrange multiplier μ that acts as second continuation parameter) is started with a trivial homogeneous solution and is switched to a branch of periodic solutions of hexagonal order after the corresponding primary pitchfork bifurcation is detected. In a secondary bifurcation a branch bifurcates that consists of nearly rotationally invariant localized targetlike
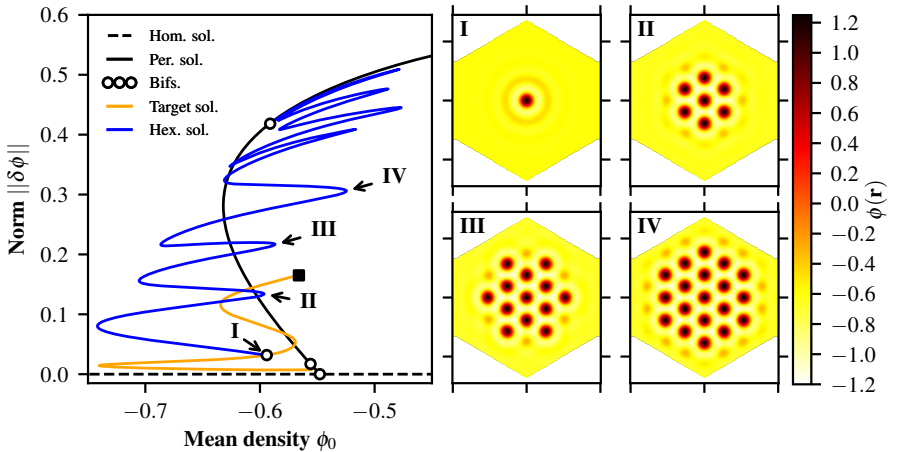
20

Figure 7: (left) Bifurcation diagram for the steady Swift-Hohenberg equation (42) with $\delta = 0$ showing slanted homoclinic snaking of localized hexagonal "crystals" at the center of a two-dimensional hexagonal domain. Shown is the norm as a function of the mean density ϕ_0, while the Lagrange multiplier μ acts as second continuation parameter. The right panel gives selected profiles at loci indicated by corresponding arrows in the left panel. Again, we set $r = -0.9$.

solutions (in a domain that does not show this symmetry). The targetlike structure grows in extension along the branch. For simplicity we only show the part of this branch where the interaction of the localized structure with the Neumann boundaries is negligible (end of shown part marked by black square symbol in fig. 7(left)). In a tertiary bifurcation localized hexagonal "crystals" emerge. Similar to the one-dimensional case shown in figs. 5 and 6, these patches grow layerwise along the branch that shows slanted snaking. Here, an intermediate state (**III**) is found between subsequent fully developed hexagons (**II** and **IV**), i.e., it takes four saddle-node bifurcations to add another layer. Further side-branches exist that are not shown here. Note that also for two-dimensional domains vertically aligned snaking is found in the case of the standard nonmass-conserving SH, i.e., eq. (42) with $\mu = 0$ and $\delta \neq 0$ [78]. Extended analyses of such localized patterns for reaction-diffusion systems in two-dimensional domains are found in [134, 136].

Remark 1. *To also compute on the fly the linear stability properties of steady states of (41) we need a slightly different splitting instead of (44), (45). We introduce two auxiliary fields $v = \Delta\phi$ and $w = \Delta v$ and consider (39) in the form*

$$0 = \Delta\phi - v \tag{46}$$
$$0 = \Delta v - w \tag{47}$$
$$\partial_t \phi = \Delta w + 2\Delta v + (1+r)\Delta\phi. \tag{48}$$

with Neumann-BC, i.e., $\nabla \cdot (v, w, \phi)^T = 0$. The FEM formulation of (48) takes the

form

$$\mathcal{M}\partial_t u = -G(u,\mu),\tag{49}$$

where $u = (u_1, u_2, u_3)$ contains the nodal values of v, w, and ϕ, respectively, and the mass matrix $\mathcal{M}$ on the left hand side has the form

$$\mathcal{M} = \begin{pmatrix} 0 & 0 & 0 \\ 0 & 0 & 0 \\ 0 & 0 & M \end{pmatrix},\tag{50}$$

where M is the one-component scalar mass matrix. The crucial point is that the eigenvalue problem $\rho\mathcal{M}v = -\partial_u G(u,\lambda)v$ for the linearization around some steady solution u then yields the correct discrete eigenvalues ρ.

5 The Kuramoto-Sivashinsky equation

The Kuramoto-Sivashinsky (KS) equation [74, 111] is a canonical and much studied nonlinear model for long-wave instabilities in dissipative systems, for instance in laminar flame propagation, or for surface waves on inclined thin liquid films [24], and is often considered as a model for spatiotemporal chaos and (interfacial) turbulence [63, 69, 98, 91, 29]. Here we consider the KS equation in the form

$$\partial_t \phi = -\sigma\partial_x^4\phi - \partial_x^2\phi - \frac{1}{2}\partial_x(\phi^2),\tag{51}$$

with parameter $\sigma > 0$, on the one-dimensional domain $x \in (-2,2)$ with periodic BC. It is obtained from Eq. (7) by neglecting nonmass-conserving contributions and nongradient contributions to the chemical potential, introducing a constant mobility in the mass-conserving flux, i.e.,

$$Q_{nc} = \mu_{nc}^{ng} = \mu_c^{ng} = 0 \quad \text{and} \quad Q_c = 1,\tag{52}$$

employing the energy functional (5) with $f(\phi) = -\frac{1}{2}\phi^2$, and the nongradient flux term of type (ii) with $n = 2$ (§1), i.e., $\mathbf{j}_c^{ng} = -\frac{1}{2}\partial_x(\phi^2, 0)^T$.

Equation (51) with periodic BC is translationally invariant, it has the boost invariance $\phi(x,t) \mapsto \phi(x-st)+s$, and thus we need the two phase conditions (14) and (15). We therefore modify (51) to

$$\partial_t \phi = -\sigma\partial_x^4\phi - \partial_x^2\phi - \frac{1}{2}\partial_x(\phi^2) + s\partial_x\phi + \varepsilon,\tag{53}$$

where the wave speed s comes from the comoving frame $x = x - st$, and the fictitious influx ε acts as the additional continuation parameter related to side condition (14). It is zero (numerically 10^{-10}) for all computations presented here. Fixing the mass to $m_0 = \int_\Omega \phi\,dx = 0$ and employing σ as primary continuation parameter, eq. (51) shows pitchfork bifurcations (pitchforks of revolution) from the trivial homogeneous solution $\phi \equiv 0$ to stationary spatially periodic solutions at $\sigma_k = (2/k\pi)^2$, $k \in \mathbb{N}$, see bifurcation diagram in fig. 8(a). Such bifurcations have been studied, e.g., in refs. [67, 29]. Following the emerging branches with decreasing σ we obtain secondary Hopf bifurcations on some branches of steady patterns, and for $\sigma \to 0$ the dynamics becomes more and more complicated, making (51) a model for (interfacial) turbulence. Ref. [16] employs time-stepper methods following [105] to determine a fairly complete bifurcation diagram for eq. (51)

(with σ in the range 0.025 to 0.4) on a domain $\Omega = (0,2)$ with *Dirichlet* BC, i.e., $\phi(0,t) = \phi(2,t) = \partial_x^2 \phi(0,t) = \partial_x^2 \phi(2,t) = 0$. In particular, many bifurcations have been explained analytically as being related to hidden symmetries made visible by antisymmetrically extending solutions onto the domain $(-2,2)$ with periodic BC (also cf. [27]).

Figure 8(a) presents basic bifurcation diagrams for (51) as determined with PDE2PATH while figs. 8(b) and 8(c) present selected corresponding profiles of steady and time-periodic solutions, respectively. As predicted, at σ_k we find supercritical pitchfork bifurcations where branches of steady periodic solutions emerge. The first one starts out stable at $\sigma_1 = 4/\pi^2 \approx 0.405$, and looses stability in another supercritical pitchfork bifurcation at about $\sigma = 0.13$ (example solution I) to a traveling wave branch (brown), which then looses stability in a Hopf bifurcation (right panel in (a), and example solution (VI)). The 2nd, 3rd and 4th steady state branches gain stability at some rather large amplitude, then loose it again in Hopf bifurcations (II and III for the 2nd and 3rd branch). The bifurcating Hopf branches consist of standing waves, start out stable but become unstable via pitchfork bifurcations. These results all fully agree with those in [16] (by antisymmetrically extending the solutions from [16]). There, they also compute some further (standing-wave) Hopf branches bifurcating in the above pitchforks and period doublings from the standing-wave Hopf branches. Here, additionally we have traveling waves and Hopf bifurcations to modulated traveling waves, with VI just one example. While Fig. 8 essentially corroborates the results of ref. [16], here the results are obtained with a few functions (implementing (51) and Jacobians) and commands within the PDE2PATH setup, see [130, §5.2] for details.

For the computation of Hopf orbits we modify eqs. (14) and (15) to

$$q_1^H(u(\cdot,\cdot)) := \sum_{i=1}^{m} \left(\int_\Omega u(t_i,x)\,\mathrm{d}x - m_0 \right) = 0, \quad q_2^H(u(\cdot,\cdot)) := \sum_{i=1}^{m-1} \langle \partial_x u^*, u(t_i) \rangle = 0,$$

where as before u denotes the spatio-temporal discretization of ϕ, and $\partial_x u^*$ is to be understood in the discrete sense. The first equation fixes the average (in t) mass to m_0, where it turns out that the mass is also conserved pointwise (in t), while the second equation fixes the *average* wave speed s.

6 Convective Allen-Cahn equation

6.1 Model

Another example of a nonvariational equation is given by a convective Allen-Cahn (cAC) equation obtained from eq. (7) neglecting mass-conserving contributions, introducing a constant mobility in the nonmass-conserving flux, i.e.,

$$Q_c = \mathbf{j}_c^{\mathrm{ng}} = 0 \quad \text{and} \quad Q_{\mathrm{nc}} = 1, \tag{54}$$

and a nongradient parity-breaking rate term $\mu_{\mathrm{nc}}^{\mathrm{ng}} = v\partial_x\phi$ that corresponds to a convective term of the form of a comoving frame term. The energy functional is as for the AC equation [eq. (23)] with

$$f(\phi) = \frac{a}{2}[1 + \xi g(x)]\phi^2 + \frac{1}{4}\phi^4, \tag{55}$$

(a) Bifurcation diagram of selected steady state and TW branches and zoom into BD with Hopf branches (left); and bifurcation of modulated TW (right).

(b) Selected steady solutions.

(c) Selected time periodic solutions (VI in a comoving frame with speed $s \approx -0.3$).
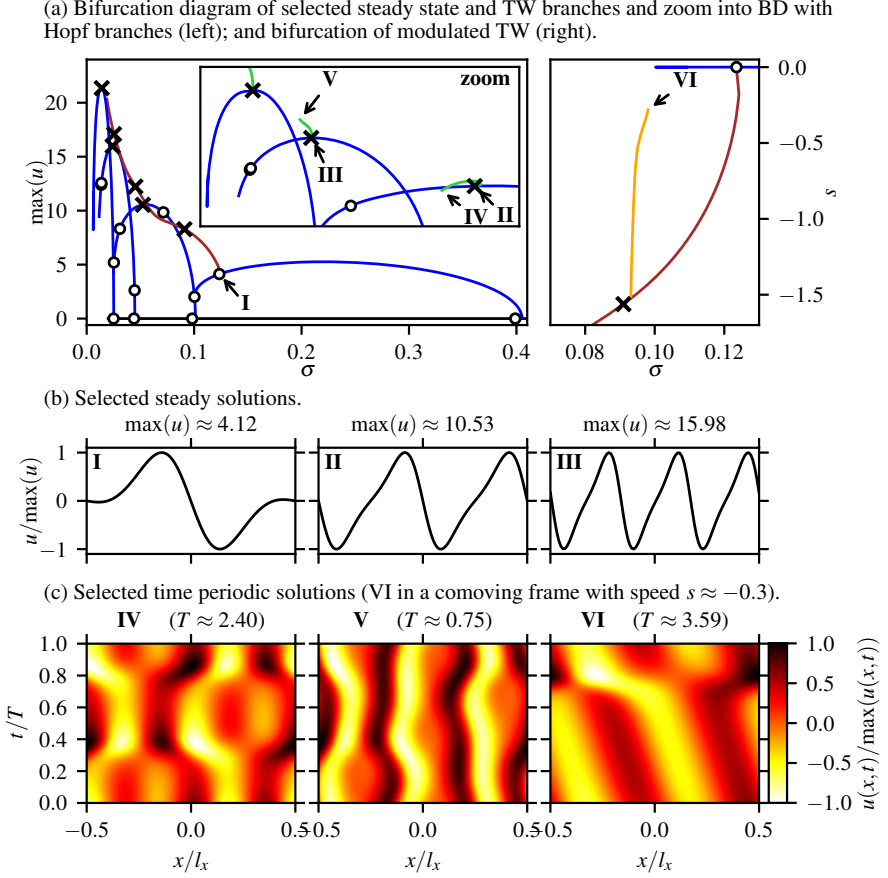
Figure 8: Partial bifurcation diagrams and selected solutions for (51). Steady bifurcations (speed $s = 0$) and bifurcations to TW ($s \neq 0$) indicated by $\circ$, Hopf bifurcations by $\times$. See main text for detailed comments.

24

i.e., allowing for a spatial variation of the destabilizing term.

Again, restricting ourselves to one-dimensional systems, the resulting equation is

$$\partial_t \phi = \sigma \partial_{xx} \phi - a(1 + \xi g(x))\phi - \phi^3 - v\partial_x \phi + \mu . \tag{56}$$

Here, the spatial modulation is given by

$$g(x) = -\tanh(x + R_s) + \tanh(x - R_s) , \tag{57}$$

i.e., $g = 0$ for $x \lesssim -R_s$ or $x \gtrsim R_s$ and $g = -2$ for $-R_s \gtrsim x \lesssim R_s$. In this setup for $a > 0$, pattern formation is possible in a defined region of length $2R_s$ (here $= l_x/3$). The model is meant to describe a very simple spatially extended system where a pinning influence (heterogeneity) and lateral driving force (convective term) compete in the vicinity of a phase transition (double well potential) of a nonconserved order parameter field. It may describe, e.g., a magnetizable foil that is dragged over a window kept at a temperature below the Curie temperature and is at higher temperature elsewhere. Then patterns of spontaneous magnetization may occur in the low-temperature region. The field μ stands for an external magnetic field.
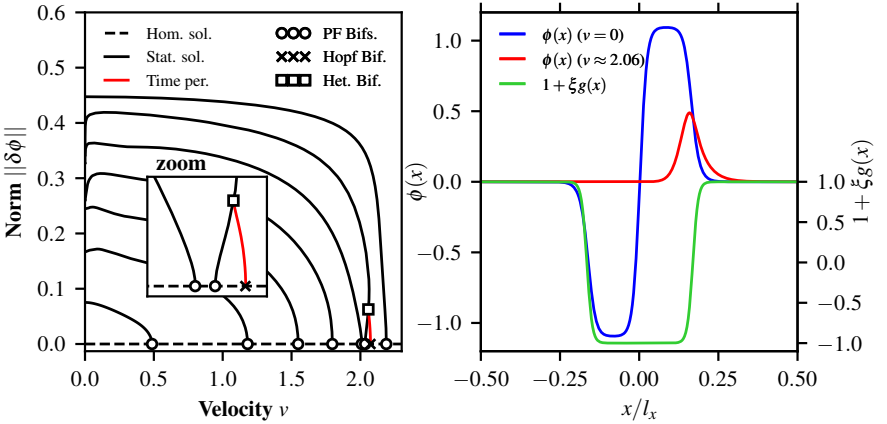
6.2 Continuation

Figure 9: (left) Bifurcation diagram and (right) selected steady modulated solution profiles (on second branch from top) for the convective Allen-Cahn equation (56) for $a = 1.2$, $\mu = 0$ and $\sigma = \xi = 1$. Homogeneous, steady modulated and time-periodic solution branches are shown in the left panel as dashed black, solid black and solid red lines, respectively. Shown is the (time-averaged) norm as a function of the speed v. Corresponding space-time plots of time-periodic solutions are given in fig. 10.

For our one-dimensional problem we use a domain $\Omega = [-l_x/2, l_x/2]$ with $l_x = 60$ and periodic boundary conditions. In contrast to §4 the explicit spatial dependency induced by the heterogeneity $g(x)$ breaks the translational symmetry, i.e., a phase condition is not needed for continuation. We fix $\sigma = \xi = 1$, $\mu = 0$ and use the speed v as the primary (and here only) continuation parameter.
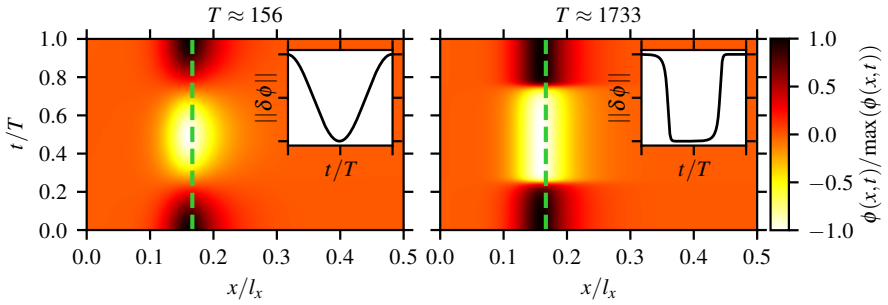
Figure 10: Space-time plots of time-periodic states on the branch of time-periodic solutions shown as solid red curve in fig. 9(left). The left panel shows a harmonic time dependence close to the Hopf bifurcation while the right panel shows a strongly unharmonic oscillation resembling switching behavior close to the global (heteroclinic) bifurcation.

The obtained bifurcation diagram for $a = 1.2$ is given in the left panel of fig. 9 while the right panel gives selected steady profiles. The homogeneous solution branch with $\partial_x \phi = 0$ exists for all values of the advection velocity v. It is linearly stable at large v and with decreasing v becomes more and more unstable at a number of pitchfork bifurcations. All emerging branches of steady spatially modulated states continue till $v = 0$ where then a number of such states exist showing structures with a different number of extrema that are confined to the patterning window. Figure 9(right) shows the profile with two extrema (blue curve), i.e., the one connected to the bifurcation at the second largest critical value of v, together with the heterogeneity profile (green curve). Whilst at $v = 0$ the solution has the odd symmetry $(x, \phi) \to (-x, -\phi)$, with increasing v the structure gets increasingly suppressed and dragged towards the right border of the patterning window (red curve). Time simulations show that only the steady modulated state of largest norm is linearly stable.

Beside the pitchfork bifurcations the trivial branch can also show Hopf bifurcations. Here, at $a = 1.2$ one Hopf bifurcation is detected at about $v = 2.07$ where a branch of time-periodic, spatially modulated solutions emerges. Close to onset they correspond to harmonic oscillations of the stationary solutions shown in fig. 9 (right panel). An example is given in the space-time plot of fig. 10(left). Moving away from onset one finds that the oscillation becomes increasingly unharmonic till finally it resembles abrupt and switches between the two steady modulated solutions that correspond to the nearby branch. [5] Decreasing v, the overall time period T increases until it diverges when the time-periodic solution ends in a global (heteroclinic) bifurcation on both symmetry-related branches of steady solutions (see inset of Figure 9(left)).

Note that changing a one can adjust the number of branches of steady modulated solutions: starting at $a = 0$ with increasing a more and more pitchfork bifur-

---

[5]Note that in the representation with the norm as solution measure each branch of inhomogenous steady states actually represents two branches related by symmetry $\phi(x) \to -\phi(x)$.

cations appear at small v and move towards larger v. Eventually, Hopf bifurcations appear together with heteroclinic bifurcations in codimension-2 Takens-Bogdanov bifurcations at the primary pitchfork bifurcations. Also the pitchfork bifurcations may interact and annihilate, thereby producing branches of steady modulated solutions not connected to the trivial branch (not shown).

7 Convective Cahn-Hilliard equation

7.1 Model

There exists a variety of systems described by convective Cahn-Hilliard (cCH) equations. They are obtained from eq. (7) neglecting nonmass-conserving contributions and nongradient chemical potentials, introducing a constant mobility in the mass-conserving flux, i.e.,

$$Q_{nc} = \mu_{nc}^{ng} = \mu_c^{ng} = 0 \quad \text{and} \quad Q_c = 1,\tag{58}$$

and a nongradient flux term $\mathbf{j}_c^{ng} = (v\phi, 0)T$ corresponding to a convective term in the form of a comoving frame term. Employing the energy functional (23) with (24) as for the standard CH equation, one has for a one-dimensional geometry

$$\partial_t \phi = -\partial_{xx}\left[\sigma\partial_{xx}\phi + \phi - \phi^3 - \mu g(x)\right] - v\partial_x \phi\tag{59}$$

where $g(x)$ is as in §6 a spatial heterogeneity

$$g(x) = -\frac{1}{2}\left[1 + \tanh\left(\frac{x - x_s}{l_s}\right)\right].\tag{60}$$

It again implies that the driving comoving frame term can not be removed by a coordinate transition as a particular frame of reference (laboratory frame) is selected by the heterogeneity.

Such equations are relevant for phase separation in dragged-plate systems like occurring in Langmuir-Blodgett transfer of surfactant monolayers from the surface of a bath onto a moving plate [115, 25]. In this context, $\mu g(x)$ is a space-dependent external field that models the interaction between the surfactant monolayer and the substrate. It describes, for instance, the substrate-mediated condensation [115] that occurs when the surfactant layer comes close to the substrate, i.e., in the transition region between the bath and the withdrawing plate with speed v (for details see Refs. [70, 71]). With other words, $g(x)$ is responsible for a space-dependent tilt of the double-well potential $f(\phi)$ (see Eq. (24).

There, in certain ranges of parameters like plate velocity and surfactant concentration, stripe patterns result that can be perpendicular or parallel to the direction of plate motion. The stripes are related to the first order phase transition in the surfactant layer that is triggered by the substrate-mediated condensation effect [115, 25]. Closely related (coupled) thin-film equations are studied in the context of dip coating with simple [113, 145, 51] (Landau-Levich systems) or complex [138] liquids and, in general, for solute deposition at receding contact lines [49, 42, 121].

Beside the presented convective CH equation (59) another class of such equations exist. They consist of Eq. (26) with an additional nonlinear driving term $\sim \partial_x \phi^2 \sim \phi \partial_x \phi$, i.e., $j_c^{ng} \sim (\phi^2, 0)^T$ [142] and model phase separation in driven systems like, for instance, phase-separating systems with concentration gradients

that cause hydrodynamic motion [55] or the faceting of growing crystal surfaces [54]. In this case the system is translation invariant.

However, here we only consider the first type of convective CH equation [eq. (59)] and emphasize that it may be seen as a generic model for many systems where a pinning influence, like a boundary or/and a heterogeneity, competes with a lateral driving force that keeps the system permanently out of equilibrium (here the plate motion) in the vicinity of a first order phase transition involving a conserved quantity (e.g., a phase transition involving a density change or a wetting transition). As a result one expects the bifurcation structure of this type of modified Cahn-Hilliard model to be of interest for a wider class of systems.

7.2 Continuation

For the numerical continuation of steady and time-periodic solutions of Eq. (59) in a domain of size L with BC

$$\phi(0) = \phi_0, \quad \partial_{xx}\phi(0) = \partial_x\phi(L) = \partial_{xx}\phi(L) = 0 \tag{61}$$

the continuous system is spatially discretized onto an equidistant grid of N points thereby approximating the PDE by a dynamical system consisting of N coupled ODEs. In Ref. [71] a second order finite difference scheme is employed to approximate spatial derivatives. For this large ODE system ($N = 100\ldots400$) the package AUTO07P can be used to continue fixed points of the dynamical system that correspond to steady solution profiles $\phi_0(x)$ of the PDE, to detect local bifurcations of the fixed points, to continue branches of time-periodic states, detect their bifurcations and to continue secondary branches of time-periodic states that emerge at period-doubling bifurcations. The time-periodic states represent the deposition of regular line patterns. Before Ref. [71] such behavior was only determined via time simulations, i.e., only branches of stable periodic deposition could be detected [70]. This is to our knowledge still the status for all other dip-coating systems.

However, the various transition scenarios between homogeneous deposition and various deposition patterns can only be understood if the complete structure of the bifurcation diagram is known including branches of unstable time-periodic states. As an example we analyze the emergence of stripe patterns using model (59) with (61) employing the described continuation method for 1d substrates.

In particular, we take the plate velocity as continuation parameter and obtain the harplike bifurcation diagram shown in fig. 11. Time-periodic states (corresponding to transfer of stripe patterns) emerge at low plate velocities through global (homoclinic or sniper) bifurcations from unstable branches or saddle-node bifurcations, respectively, of steady profiles that form part of a snaking family of steady states (for details see caption of Fig. 11). At high plate velocities the time-periodic solutions emerge through a number of sub- and supercritical Hopf-bifurcations. Period-doubling bifurcations are also involved.

Beside detecting the bifurcations and following all branches of steady and time-periodic states, AUTO07P also allows one to track the loci of the various bifurcations in appropriate two-parameter planes and thereby directly determine morphological phase diagrams. Fig. 12 illustrates that this is also possible for the large system of ODEs resulting from the discretization of the PDE (59). However, the continuation sometimes becomes "fragile" and at points has to be restarted with adjusted tolerances etc. With the present methods it is not yet possible to unambiguously identify the potential Bogdanov-Takens points where a homoclinic and
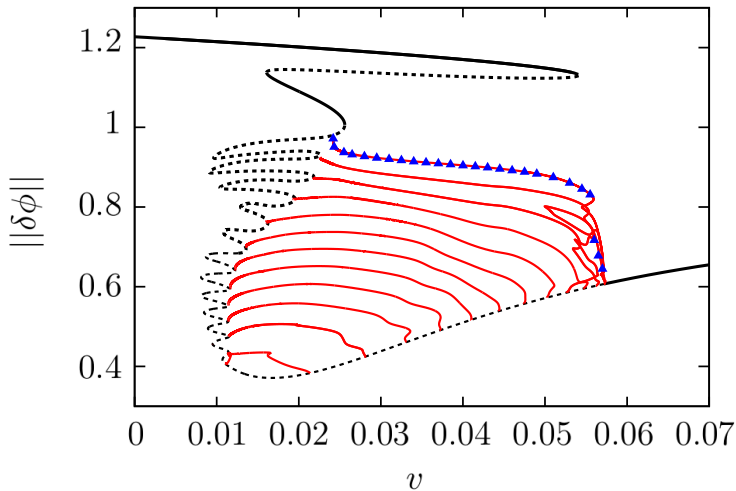
Figure 11: Harplike bifurcation diagram for the Langmuir-Blodgett transfer system. Shown is the (time-averaged) norm $||\delta\phi||$ of steady and time-periodic solutions of Eq. (59) with (61) in dependence of the dimensionless plate velocity v for domain size $L = 100$ and $\sigma = 1.0$. For remaining parameters see ref. [71]. The solid and dashed black lines represent stable (corresponding to homogeneous transfer) and unstable steady profiles, respectively, and the thin solid red lines represent time-periodic solutions (corresponding to transfer of stripe patterns), all as obtained by numerical path continuation with AUTO07P. The blue triangles correspond to time-periodic solutions obtained by direct numerical simulation [70]. For movies of time-periodic solutions see supplementary material of [71]. Figure adapted from Ref. [71].
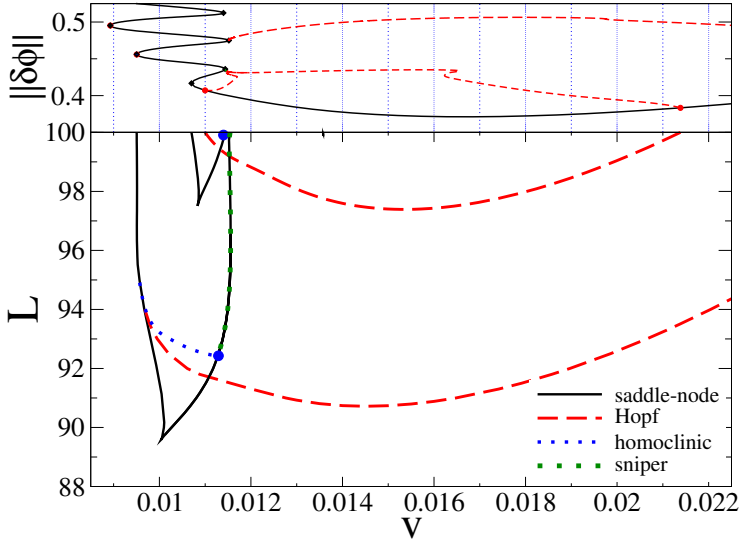
Figure 12: Two-parameter continuation of loci of bifurcations: The upper panel shows a zoom onto the tip of the harplike bifurcation diagram in fig. 11 showing all bifurcations at domain size $L = 100$ that are continued in the plane spanned by plate velocity v and L shown in the lower panel. Note that in the chosen parametrization L can be considered as a measure of the distance to the critical point of the underlying first order phase transition [71]. In particular, we show loci of four saddle-node bifurcations (black solid lines), four Hopf bifurcations (red dashed lines), and of the homoclinic [sniper] bifurcation where one of the branches of time-periodic states terminates (thin [thick] dotted line). Blue filled circles indicate where a homoclinic and a sniper bifurcation are created through the collision of a branch of time-periodic states with one of steady states. Above the lower filled circle a sniper bifurcation coincides with the black solid line of the respective fold. Figure adapted from Ref. [71].

a Hopf bifurcation emerge/annihilate (on the leftmost saddle-node bifurcation in Fig. 12).

For the future, the techniques and investigations should undergo a major extension towards the case of 2d substrates where transitions between the various different patterns could not yet been investigated by continuation methods and are, in general, still rather poorly understood although many experimental results exist [121]. Such studies should be performed for reduced models like Eq. (59), but also for the hydrodynamic thin-film models occurring in the wider class of dip-coating and receding-contact-line deposition systems [121, 49, 42, 138].

For spatially periodic systems, another way of approximating a PDE to a finite set of ODEs shows better results, i.e., needs fewer ODEs. Namely, the solution is expressed in the form of a truncated Fourier series with time-dependent coefficients that are the independent variables of the resulting dynamical system. Coupling the package AUTO07P with a fast Fourier transformation package, the scheme is used to study depinning droplets on the outside of a rotating cylinder [77] and spiral waves in reaction-diffusion systems [13]. It may also be applied to nonlocal (integro-differential) equations, e.g., applying numerical continuation to obtain bifurcation diagrams for dynamical density functional theories (DDFT), e.g., for steady states of (potentially coarsening) clusters of interacting particles in corrugated nanopores [100], and steady and time-periodic states in a model for the transport of clusters through such pores [99].

8 Nonvariational thin-film equation

8.1 Model

The previous two sections have analyzed pattern formation in driven AC and CH equations as examples of nonvariational models with nonmass-conserving and mass-conserving dynamics, respectively, using spatially one-dimensional settings. We next investigate a nonvariational thin-film (TF) equation modeling sliding drops on a two-dimensional inclined substrate. They are obtained from eq. (7) neglecting nonmass-conserving contributions and nongradient chemical potentials, introducing a nonconstant nonlinear mobility in the mass-conserving flux, i.e.,

$$Q_{nc} = \mu_{nc}^{ng} = \mu_c^{ng} = 0 \quad \text{and} \quad Q_c = \frac{\phi^3}{3}. \tag{62}$$

and a driving nongradient flux term $\mathbf{j}_c^{ng} = G_0 \alpha \frac{1}{3}(\phi^3, 0)^T$. Here, $\phi(\mathbf{r},t)$ is the two-dimensional height profile of a three-dimensional liquid film. To model contributions of Laplace and Derjaguin pressure as well as the hydrostatic pressure proportional to the gravity number G_0, we define the energy functional as

$$\mathscr{F}[\phi] = \int_\Omega \frac{\sigma}{2} (\nabla \phi)^2 + f(\phi) + \frac{1}{2} G_0 \phi^2 \, d\mathbf{r} \tag{63}$$

where the nongravitational bulk energy $f(\phi)$ is given by the wetting potential (32) in §32. Note that by setting $Q_{nc} \neq 0$ and $\mu_{nc}^g \neq 0$ a simple evaporation model may be incorporated [120, 121]. The corresponding PDE is then given by

$$\partial_t \phi = -\nabla \cdot \left[\frac{\phi^3}{3} \nabla \underbrace{\left(\sigma \Delta \phi + \left[-\phi^{-3} + \phi^{-6} \right] - G_0 \phi \right)}_{=p} + G_0 \alpha \frac{1}{3}(\phi^3, 0)^T \right]. \tag{64}$$

where we introduced the pressure p. This equation may also be derived via a long-wave approximation of the Navier-Stokes equations with suitable boundary conditions [94, 119]. As any nonzero inclination angle will cause liquid structures to slide down the substrate, to study stationary moving drops we further transform eq. (64) into the frame moving with the sliding velocity U. The stationary equation is

$$0 = -\nabla \cdot \left[\frac{\phi^3}{3} \nabla p + G_0 \alpha \frac{1}{3}(\phi^3, 0)^T - U(\phi, 0)^T \right]. \tag{65}$$

Defining the new field $u = p + G_0 \phi$, eq. (65) is split into two second order equations

$$0 = u - \sigma \Delta \phi - \left[-\phi^{-3} + \phi^{-6} \right] \tag{66}$$

$$0 = -\nabla \cdot \left[\frac{\phi^3}{3} \nabla(u - G_0 \phi) + G_0 \alpha \frac{1}{3}(\phi^3, 0)^T - U(\phi, 0)^T \right] + \varepsilon \tag{67}$$

Note that for a dragged film system, eq. (67) is still valid in the laboratory frame with U representing driving due to the drag of the moving plate that is inclined by the angle α (analogue to eq. (59) in §7).
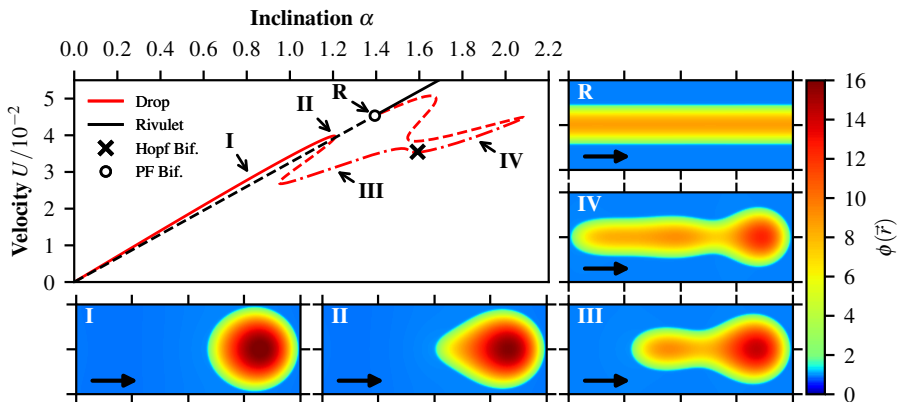
8.2   Continuation

Figure 13: (top left) Bifurcation diagram for and (left and bottom) selected corresponding profiles of sliding drops on a domain $l_x \times l_y$ with $l_x = 4l_y = 200$, $\alpha = 0.5$, $\sigma = 1.0$ and Neumann BCs. The bifurcation diagram gives the drop velocity in dependence of plate inclination. Stable and unstable solutions are given as solid and dashed lines, respectively.

In contrast to §3.3, here, the drop volume or mean film height can not be imposed via a Lagrange multiplier as it only appears in the steady state equation (34) after two integrations, i.e., is not applicable for the present nonvariational system. Here, we use PDE2PATH to continue the out of equilibrium system (67) with integral side conditions for volume conservation (eq. (14)) and the phase condition

32

(eq. (15)) needed due to the periodic boundary conditions in x-direction. For the two resulting additional continuation parameters we follow the scheme of §5, i.e., we use the sliding velocity U and a fictitious homogeneous influx ε (that is then kept at zero by the continuation). In y-direction we split the physical domain given by $l_x \times l_y = 200 \times 100$ in half and employ Neumann BC in analogy to §3.3.

As starting solution we employ a single steady drop on a horizontal substrate ($\alpha = 0$) similar to profile **D**1 in fig. 3. Employing the inclination angle α as primary continuation parameter we obtain the bifurcation diagram in fig. 13 (top left). Selected corresponding profiles are given in the other panels. At relatively small α, the branch represents linearly stable sliding drops (example profile **I**) with a nearly linear $U(\alpha)$ dependence. This sub-branch ends in a saddle-node bifurcation at a critical inclination α_c (example profile **II**). The branch destabilizes and turns back towards smaller α, i.e., a subbranch of linearly unstable profiles coexists with the stable one. At another saddle-node bifurcation the branch turns again towards larger α and passes through some further saddle-node bifurcations before joining the branch of rivulet solutions of equal volume (example profile **R**) in a pitchfork bifurcation (in the comoving frame). Note that in the laboratory frame this bifurcation is seen as a traveling wave bifurcation. Along the branch of drop solutions further real and/or complex eigenvalues destabilize and stabilize depending of the exact parameter values and details of the model (cf. [46, 137]). In all cases, beginning at about the first saddle-node bifurcation, the drop profiles develop an elongation at their rear end (example profiles **III** and **IV**).

A detailed analysis of this system is given in ref. [46] where the hydrostatic pressure term is neglected. Information from bifurcation diagrams as fig. 13(top left) may be employed to predict the statistical behavior of ensembles of sliding drops when 'fed into' a Smoluchowski-type statistical model for the distribution of drop volumes in large ensembles of interacting sliding drops [137].

Finally, we briefly discuss the above mentioned related system of dip coating that is also described by eq. (65): a solid substrate is drawn with velocity U out of a liquid bath deforming the liquid meniscus or dragging a Landau-Levich film onto the moving plate [113, 145, 51, 139]. The upper right panel of fig. 14 shows typical dragged meniscus profiles and acts as a sketch of the system. To determine steady solutions of the dragged plate problem with eq. (67), the boundary conditions (BC) in x-direction have to be changed and both integral side conditions can be dropped as translation symmetry is broken by the BC and the liquid volume is controlled by the influx given through the BC at the side of the bath. Continuation has been employed in the literature to obtain bifurcation diagrams for one-dimensional substrates using AUTO07P [51], while here we present first PDE2PATH results for fully two-dimensional substrates. Then, transversal instabilities are possible, i.e., the contact line between bath and plate does not need to remain straight.

In our geometry, the bath is on the right hand side, i.e., the plate is withdrawn towards the negative x-direction. The particular BC used are on the one hand, Neumann BCs for both fields at the left boundary end ($x = -l_x/2$) where an ultrathin adsorption layer or macroscopic Landau-Levich film is drawn out. On the other hand, at the liquid bath ($x = l_x/2$) we employ Dirichlet BC for the height field ϕ (for the shown runs $\phi(l_x/2) \approx 44$) and Neumann BC for the second field u, i.e., we impose conditions on ϕ and $\partial_x^3 \phi$. We employ Neumann BC in the y-direction. Figure 14(left) gives the bifurcation diagram for fixed inclination $\alpha = 0.5$ using the plate velocity U as continuation parameter. The dashed line reproduces the
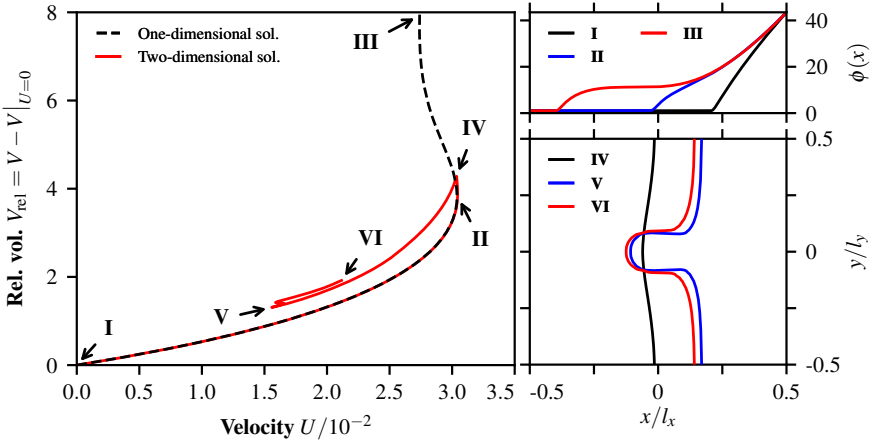
33

Figure 14: Bifurcation diagram (left) and solution profiles (right) for a solid substrate pulled out of a liquid bath with $l_x = 250$, $l_y = 220$ and $\sigma = 1.0$. Both, the explicit one dimensional (top right) and the two dimensional case (bottom right) are shown. In the latter case the black, blue and red lines visualize the contact lines of the liquid defined by the condition $\phi(\mathbf{r}) = 1.5$.

result of Ref. [128] for a one-dimensional substrate, i.e., the curve for profiles $\phi(x)$ that in a two-dimensional setting represent solutions that are translationally invariant in the transversal y-direction. In contrast, the solid red line gives the fully two-dimensional result. Initially, at small U the two cases are identical, but then slightly above the saddle-node bifurcation a pitchfork bifurcation occurs where solutions with transversally modulated profiles emerge. Examples of "contact lines" are shown in the lower right panel of fig. 14. At first the modulation is harmonic to then become strongly nonlinear and localized at the center. The branch undergoes further saddle-node bifurcations that shall be further investigated in the future.

9   Conclusions

In the present chapter we have given an overview of the application of continuation techniques to a class of nonlinear kinetic equations (1) for single scalar order parameter fields. First, we have introduced a general classification of these equations by distinguishing (i) mass-conserving and nonmass-conserving dynamics, and (ii) gradient (variational) and nongradient (nonvariational) dynamics resulting in the general form eq. (7). Furthermore, we have distinguished different types of energy functionals underlying the variational part of the dynamics. As a result the chapter covers Allen-Cahn- and Cahn-Hilliard-type equations (including thin-film equations) as well as Swift-Hohenberg and Phase-Field-Crystal equations – most of them in their 'pure' variational form and also with various nonvariational extensions that we also classify. Second, we have briefly reviewed the technique of numerical (pseudo-)arclength continuation and the structure of the corresponding

numerical algorithms that are employed in the packages AUTO07P and PDE2PATH.

In the main part we have given various examples that illustrate how continuation techniques are applied in the investigation of particular physical problems modeled by the introduced equations. For each example we have discussed the specific equation, boundary conditions and integral side conditions and have laid out any resulting implementation issues. Particular emphasis has been put on explaining the number, kind and physical meaning of the various employed continuation parameters. Results have been shown and discussed in the form of selected bifurcation diagrams and solution profiles referring the reader for further details and results to the literature.

In particular, §3 has started with the rather simple example of a pure gradient dynamics of Allen-Cahn type. It has been employed to illustrate the calculation of branches of steady state solutions of PDEs without any side conditions. We have then explained how these branches relate to solutions of Cahn-Hilliard-type equations that imply a side condition related to mass conservation. Next, we have considered in §4 branches of steady state solutions of the Swift-Hohenberg and Phase-Field-Crystal equations this time employing periodic boundary conditions. The latter request a phase condition as integral side condition that breaks the translational invariance and implies the usage of an additional continuation parameter that represents a fictitious advection. As the corresponding steady PDEs are of fourth order we have discussed both, the concept of splitting a system in multiple second order equations and directly implementing a fourth order equation in PDE2PATH. Examples have been given in one and two dimensions and the relation between the steady solutions of both equations has been discussed.

The remaining sections have discussed equations with nonvariational parts. First, §5 has analyzed the Kuramoto-Sivashinsky equation and has introduced the ability of PDE2PATH to detect Hopf bifurcations and to continue emerging branches of time-periodic solutions, namely, travelling and modulated waves. In §6 and 7 we have then presented results for nonvariational forms of the Allen-Cahn and Cahn-Hilliard equation, respectively, in cases where an explicit spatial dependency exist. These sections also contain examples for the detection of Hopf-bifurcations and continuation of emerging branches with both, PDE2PATH and AUTO07P, in part involving period-doubling bifurcations of time-periodic states and global bifurcations. Section §8 has then dealt with two nonvariational forms of the thin-film equation describing drops sliding on an incline and a dragged meniscus problem, respectively.

The chapter has laid out the present state of the art of the application of continuation techniques to the class (7) of nonlinear kinetic equations for one- and two-dimensional domains. While we have focused on such equations for a single scalar field, there are many more related equations when allowing for several coupled scalar fields [47, 68, 26, 89, 60, 87, 107, 90, 122] or indeed coupled scalar, vector and tensor fields [114, 85, 95]. Complicated problems involving several scalar fields are dealt with in many of the tutorials and demos coming with PDE2PATH, and research papers using PDE2PATH, in 1d, 2d and 3d, for instance

- reaction-diffusion systems in [135, §4], [132] and, mostly ecology related, in [134, 110, 136, 143], including some optimal control aspects [129], [132, §3.4];

- Bose-Einstein condensates [39, 40], Rayleigh-Benard convection and related fluid problems [135, §5], [144];

- Poisson-Nernst-Planck systems, i.e., ionic liquids in [10, 52];
- Laser dynamics systems in [58, 106].

There are a few works where continuation is applied to models that couple scalar fields to vector fields [104, 34] (also consider ref. [90, 105] for more details on the used techniques).

Note that also the continuation of branches of time-periodic solutions in 2d and 3d is still somewhat delicate in PDE2PATH, in particular with constraints such as mass conservation and phase conditions. An example is given by the Hopf bifurcation that has been detected in the sliding drop system shown in fig. 13. In ref. [46] the dynamics near the bifurcation is already studied by direct time simulations that indicate that the bifurcation is subcritical, but the continuation of the branch quickly leads to numerical problems. Here, we may need to switch to shooting based methods as in [105]. Also, bifurcations from periodic orbits still await implementation, and the numerical linear algebra can and will be improved at several places.

Acknowledgements

References

[1] Achim, C.V., Ramos, J.A.P., Karttunen, M., Elder, K.R., Granato, E., Ala-Nissila, T., Ying, S.C.: Nonlinear driven response of a phase-field crystal in a periodic pinning potential. Phys. Rev. E **79**, 011,606 (2009)

[2] Alfaro, C., Depassier, M.: A 5-mode bifurcation-analysis of a kuramoto-Sivashinsky equation with dispersion. Phys. Lett. A **184**, 184–189 (1994)

[3] Allen, S., Cahn, J.: Microscopic theory for antiphase boundary motion and its application to antiphase domain coarsening. Acta Metall. Mater. **27**, 1085–1095 (1979)

[4] Allgower, E.L., Georg, K.: Introduction to Numerical Continuation Methods (Classics in Applied Mathematics). Society for Industrial Mathematics (1987)

[5] Alvarez-Socorro, A., Clerc, M., Gonzalez-Cortes, G., Wilson, M.: Nonvariational mechanism of front propagation: Theory and experiments. Phys. Rev. E **95**, 010,202 (2017)

[6] Archer, A.J., Rauscher, M.: Dynamical density functional theory for interacting brownian particles: Stochastic or deterministic? J. Phys. A-Math. Gen. **37**, 9325–9333 (2004)

[7] Archer, A.J., Robbins, M.J., Thiele, U., Knobloch, E.: Solidification fronts in supercooled liquids: How rapid fronts can lead to disordered glassy solids. Phys. Rev. E **86**, 031,603 (2012)

[8] Avitabile, D., Lloyd, D., Burke, J., Knobloch, E., Sandstede, B.: To snake or not to snake in the planar Swift-Hohenberg equation. SIAM J. Appl. Dyn. Syst. **9**, 704–733 (2010)

[9] Bestehorn, M., Merkt, D.: Regular surface patterns on Rayleigh-Taylor unstable evaporating films heated from below. Phys. Rev. Lett. **97**, 127,802 (2006)

[10] Bier, S., Gavish, N., Uecker, H., Yochelis, A.: Mean field approach to first and second order phase transitions in ionic liquids. Phys. Rev. E **95**, 060,201 (2017)

[11] Bindel, D., Friedman, M., Govaerts, W., Hughes, J., Kuznetsov, Y.: Numerical computation of bifurcations in large equilibrium systems in matlab. J. Comput. Appl. Math. **261**, 232–248 (2014)

[12] Bonn, D., Eggers, J., Indekeu, J., Meunier, J., Rolley, E.: Wetting and spreading. Rev. Mod. Phys. **81**, 739–805 (2009)

[13] Bordyugov, G., Engel, H.: Continuation of spiral waves. Physica D **228**, 49–58 (2007)

[14] Bortolozzo, U., Clerc, M., Residori, S.: Local theory of the slanted homoclinic snaking bifurcation diagram. Phys. Rev. E **78**, 036,214 (2008)

[15] Bribesh, F.A.M., Frastia, L., Thiele, U.: Decomposition driven interface evolution for layers of binary mixtures: Iii. two-dimensional steady film states. Phys. Fluids **24**, 062,109 (2012)

[16] Buono, P.L., van Veen, L., Frawley, E.: Hidden symmetry in a Kuramoto-Sivashinsky initial-boundary value problem. Int. J. Bifurcation Chaos **27**(9), 1750,136 (2017)

[17] Burke, J., Dawes, J.: Localized states in an extended swift-hohenberg equation. SIAM J. Appl. Dyn. Syst. **11**, 261–284 (2012)

[18] Burke, J., Houghton, S., Knobloch, E.: Swift-hohenberg equation with broken reflection symmetry. Phys. Rev. E **80**, 036,202 (2009)

[19] Burke, J., Knobloch, E.: Localized states in the generalized Swift-Hohenberg equation. Phys. Rev. E **73**, 056,211 (2006)

[20] Burke, J., Knobloch, E.: Homoclinic snaking: Structure and stability. Chaos **17**, 037,102 (2007)

[21] Cahn, J.W.: Phase separation by spinodal decomposition in isotropic systems. J. Chem. Phys. **42**, 93–99 (1965)

[22] Cahn, J.W., Hilliard, J.E.: Free energy of a nonuniform system. 1. Interfacial free energy. J. Chem. Phys. **28**, 258–267 (1958)

[23] Cates, M., Tailleur, J.: Motility-induced phase separation. Annu. Rev. Condens. Matter Phys. **6**, 219–244 (2015)

[24] Chang, H.C.: Wave evolution on a falling film. Ann. Rev. Fluid Mech. **26**, 103–136 (1994)

[25] Chen, X.D., Lu, N., Zhang, H., Hirtz, M., Wu, L.X., Fuchs, H., Chi, L.F.: Langmuir-blodgett patterning of phospholipid microstripes: Effect of the second component. J. Phys. Chem. B **110**, 8039–8046 (2006)

[26] Craster, R.V., Matar, O.K.: Dynamics and stability of thin liquid films. Rev. Mod. Phys. **81**, 1131–1198 (2009)

[27] Crawford, J.D., Golubitsky, M., Gomes, M.G.M., Knobloch, E., Stewart, I.M.: Boundary conditions as symmetry constraints. In: M. Roberts, I. Stewart (eds.) Singularity Theory and its Applications, Part II, *Lecture Notes in Mathematics*, vol. 1463, pp. 63–79. Springer, New York (1991)

[28] Cross, M.C., Hohenberg, P.C.: Pattern formation out of equilibrium. Rev. Mod. Phys. **65**, 851–1112 (1993)

[29] Cvitanović, P., Davidchack, R.L., Siminos, E.: On the state space geometry of the Kuramoto-Sivashinsky flow in a periodic domain. SIAM J. Appl. Dyn. Syst. **9**(1), 1–33 (2010)

[30] Dankowicz, H., Schilder, F.: Recipes for continuation, *Comp. Sc. & Eng.*, vol. 11. SIAM (2013). See also `http://sourceforge.net/projects/cocotools/` (last accessed 02/25/18)

[31] Dawes, J.H.P.: Localized pattern formation with a large-scale mode: Slanted snaking. SIAM J. Appl. Dyn. Syst. **7**, 186–206 (2008)

[32] Dhooge, A., Govaerts, W., Kuznetsov, Y.: MATCONT: a matlab package for numerical bifurcation analysis of ODEs. ACM Trans. Math. Software **29**, 141–164 (2003)

[33] Dhooge, A., Govaerts, W., Kuznetsov, Y., Mestrom, W., Riet, A.: CL_MATCONT (2008). `www.sourceforge.net/projects/matcont/` (last accessed 02/25/18)

[34] Dijkstra, H.A., Wubs, F.W., Cliffe, A.K., Doedel, E., Dragomirescu, I., Eckhardt, B., Gelfgat, A.Y., Hazel, A.L., Lucarini, V., Salinger, A.G., Phipps, E.T., Sanchez-Umbria, J., Schuttelaars, H., Tuckerman, L.S., Thiele, U.: Numerical bifurcation methods and their application to fluid dynamics: Analysis beyond simulation. Commun. in Comp. Physics **15**, 1–45 (2014)

[35] Doedel, E.J., Champneys, A.R., Fairgrieve, T.F., Kuznetsov, Y.A., Sandstede, B., Wang, X.: AUTO: Continuation and bifurcation software for ordinary differential equations (with HomCont) (1997). `http://indy.cs.concordia.ca/auto/` (last accessed 02/25/18)

[36] Doedel, E.J., Keller, H.B., Kernevez, J.P.: Numerical analysis and control of bifurcation problems (I) Bifurcation in finite dimensions. Int. J. Bifurc. Chaos **1**, 493–520 (1991)

[37] Doedel, E.J., Keller, H.B., Kernevez, J.P.: Numerical analysis and control of bifurcation problems (II) Bifurcation in infinite dimensions. Int. J. Bifurc. Chaos **1**, 745–72 (1991)

[38] Doedel, E.J., Oldeman, B.E.: AUTO07p: Continuation and bifurcation software for ordinary differential equations. Concordia University, Montreal (2009)

[39] Dohnal, T., Siegl, P.: Bifurcation of eigenvalues in nonlinear problems with antilinear symmetry. J. Math. Phys. **57**, 093,502 (2016)

[40] Dohnal, T., Uecker, H.: Bifurcation of Nonlinear Bloch waves from the spectrum in the nonlinear Gross-Pitaevskii equation. J. Nonlinear Sci. **26**(3), 581–618 (2016)

[41] Doi, M.: Soft Matter Physics. Oxford University Press, Oxford (2013)

[42] Doumenc, F., Guerrier, B.: Self-patterning induced by a solutal Marangoni effect in a receding drying meniscus. Europhys. Lett. **103**, 14,001 (2013)

[43] Elder, K.R., Grant, M.: Modeling elastic and plastic deformations in nonequilibrium processing using phase field crystals. Phys. Rev. E **70**, 051,605 (2004)

[44] Emmerich, H., Löwen, H., Wittkowski, R., Gruhn, T., Toth, G., Tegze, G., Granasy, L.: Phase-field-crystal models for condensed matter dynamics on atomic length and diffusive time scales: an overview. Adv. Phys. **61**, 665–743 (2012)

[45] Engelnkemper, S.: Nonlinear analysis of physicochemically driven dewetting – statics and dynamics. Ph.D. thesis, Westfälische Wilhelms-Universität Münster (2017)

[46] Engelnkemper, S., Wilczek, M., Gurevich, S.V., Thiele, U.: Morphological transitions of sliding drops - dynamics and bifurcations. Phys. Rev. Fluids **1**, 073,901 (2016)

[47] Fischer, H.P., Dieterich, W.: Early-time kinetics of ordering in the presence of interactions with a concentration field. Phys. Rev. E **56**, 6909–6916 (1997)

[48] Formica, G., Arena, A., Lacarbonara, W., Dankowicz, H.: Coupling FEM with parameter continuation for analysis of bifurcations of periodic responses in nonlinear structures. J. Comput. Nonlinear. Dyn. **8**(2) (2012)

[49] Frastia, L., Archer, A.J., Thiele, U.: Modelling the formation of structured deposits at receding contact lines of evaporating solutions and suspensions. Soft Matter **8**, 11,363–11,386 (2012)

[50] Frisch, U., Bec, J.: Burgulence. In: M. Lesieur, A. Yaglom, F. David (eds.) New trends in turbulence Turbulence: nouveaux aspects, *Les Houches - Ecole d'Ete de Physique Theorique*, vol. 74, pp. 341–383. Springer Berlin Heidelberg (2001)

[51] Galvagno, M., Tseluiko, D., Lopez, H., Thiele, U.: Continuous and discontinuous dynamic unbinding transitions in drawn film flow. Phys. Rev. Lett. **112**, 137,803 (2014)

[52] Gavish, N.: Poisson–nernst–planck equations with steric effects—nonconvexity and multiple stationary solutions. Physica D **368**, 50–65 (2018)

[53] de Gennes, P.G.: Wetting: Statics and dynamics. Rev. Mod. Phys. **57**, 827–863 (1985)

[54] Golovin, A.A., Nepomnyashchy, A.A., Davis, S.H., Zaks, M.A.: Convective Cahn-Hilliard models: From coarsening to roughening. Phys. Rev. Lett. **86**, 1550–1553 (2001)

[55] Golovin, A.A., Pismen, L.M.: Dynamic phase separation: From coarsening to turbulence via structure formation. Chaos **14**, 845–854 (2004)

[56] Gomez-Solano, J.R., Boyer, D.: Coarsening in potential and nonpotential models of oblique stripe patterns. Phys. Rev. E **76**, 041,131 (2007)

[57] Govaerts, W.: Numerical methods for bifurcations of dynamical equilibria. SIAM (2000)

[58] Gurevich, S.V., Javaloyes, J.: Spatial instabilities of light bullets in passively-mode-locked lasers. Phys. Rev. A **96**, 023,821 (2017)

[59] Hazel, A., Heil, M.: oomph-lib (2017). `http://oomph-lib.maths.man.ac.uk/doc/html` (last accessed 02/25/18)

[60] Hirose, Y., Komura, S., Andelman, D.: Concentration fluctuations and phase transitions in coupled modulated bilayers. Phys. Rev. E **86**, 021,916 (2012)

[61] Houghton, S., Knobloch, E.: Swift-hohenberg equation with broken cubic-quintic nonlinearity. Phys. Rev. E **84**, 016,204 (2011)

[62] Hyman, J.M., Nicolaenko, B.: The Kuramoto-Sivashinsky equation - A bridge between PDEs and dynamical systems. Physica D **18**, 113–126 (1986)

[63] Jolly, M.S., Kevrekidis, I.G., Titi, E.S.: Approximate inertial manifolds for the Kuramoto-Sivashinsky equation - analysis and computations. Physica D **44**, 38–60 (1990)

[64] Kardar, M., Parisi, G., Zhang, Y.C.: Dynamic scaling of growing interfaces. Phys. Rev. Lett. **56**(9), 889–892 (1986)

[65] Keller, H.: Numerical solution of bifurcation and nonlinear eigenvalue problems. Application of bifurcation theory, Proc. Adv. Semin., Madison/Wis. 1976, 359–384 (1977)

[66] Keller, H.B.: Lectures on numerical methods in bifurcation problems, *Tata Institute of Fundamental Research Lectures on Mathematics and Physics*, vol. 79. Springer-Verlag, Berlin (1987)

[67] Kevrekidis, I.G., Nicolaenko, B., Scovel, J.C.: Back in the saddle again - a computer-assisted study of the Kuramoto-Sivashinsky equation. SIAM J. Appl. Math. **50**, 760–790 (1990)

[68] Kliakhandler, I.L.: Long interfacial waves in multilayer thin films and coupled Kuramoto-Sivashinsky equations. J. Fluid Mech. **391**, 45–65 (1999)

[69] Kliakhandler, I.L.: Inverse cascade in film flows. J. Fluid Mech. **423**, 205–225 (2000)

[70] Köpf, M.H., Gurevich, S.V., Friedrich, R., Thiele, U.: Substrate-mediated pattern formation in monolayer transfer: a reduced model. New J. Phys. **14**, 023,016 (2012)

[71] Köpf, M.H., Thiele, U.: Emergence of the bifurcation structure of a Langmuir-Blodgett transfer model. Nonlinearity **27**, 2711–2734 (2014)

[72] Kozyreff, G., Tlidi, M.: Nonvariational real Swift-Hohenberg equation for biological, chemical, and optical systems. Chaos **17**, 037,103 (2007)

[73] Krauskopf, B., Osinga, H.M., Galan-Vioque, J. (eds.): Numerical Continuation Methods for Dynamical Systems. Springer, Dordrecht (2007)

[74] Kuramoto, Y., Tsuzuki, T.: Persistent propagation of concentration waves in dissipative media far from thermal equilibrium. Prog. Theoret. Phys. **55**, 356–369 (1976)

[75] Kuznetsov, Y.A.: Elements of Applied Bifurcation Theory, 3rd edn. Springer, New York (2010)

[76] Langer, J.S.: An introduction to the kinetics of first-order phase transitions. In: C. Godreche (ed.) Solids far from Equilibrium, pp. 297–363. Cambridge University Press (1992)

[77] Lin, T.S., Rogers, S., Tseluiko, D., Thiele, U.: Bifurcation analysis of the behavior of partially wetting liquids on a rotating cylinder. Phys. Fluids **28**, 082,102 (2016)

[78] Lloyd, D.J.B., Sandstede, B., Avitabile, D., Champneys, A.R.: Localized hexagon patterns of the planar Swift-Hohenberg equation. SIAM J. Appl. Dyn. Syst. **7**, 1049–1100 (2008)

[79] Lust, K.: Continuation and bifurcation analysis of periodic solutions of partial differential equations. In: D. Henry, A. Bergeon (eds.) Continuation methods in fluid dynamics (Aussois, 1998), *Notes Numer. Fluid Mech.*, vol. 74, pp. 191–202. Vieweg, Braunschweig (2000)

[80] Maier-Paape, S., Miller, U., Mischaikow, K., Wanner, T.: Rigorous numerics for the cahn-hilliard equation on the unit square. Rev. Mat. Complut. **21**, 351–426 (2008)

[81] Maier-Paape, S., Mischaikow, K., Wanner, T.: Structure of the attractor of the cahn-hilliard equation on a square. Int. J. Bifurc. Chaos **17**, 1221–1263 (2007)

[82] Makrides, E., Sandstede, B.: Predicting the bifurcation structure of localized snaking patterns. Physica D **268**, 59–78 (2014)

[83] Marconi, U.M.B., Tarazona, P.: Dynamic density functional theory of fluids. J. Phys.-Condes. Matter **12**, A413–A418 (2000)

[84] Mei, Z.: Numerical bifurcation analysis for reaction-diffusion equations. Springer (2000)

[85] Menzel, A., Löwen, H.: Traveling and resting crystals in active systems. Phys. Rev. Lett. **110**, 055,702 (2013)

[86] Mitlin, V.S.: Dewetting of solid surface: Analogy with spinodal decomposition. J. Colloid Interface Sci. **156**, 491–497 (1993)

[87] Morales, M., Rojas, J., Torres, I., Rubio, E.: Modeling ternary mixtures by mean-field theory of polyelectrolytes: Coupled ginzburg-landau and swift-hohenberg equations. Physica A **391**, 779–791 (2012)

[88] Münch, A.: Pinch-off transition in Marangoni-driven thin films. Phys. Rev. Lett. **91**, 016,105 (2003)

[89] Náraigh, L.Ó., Thiffeault, J.L.: Nonlinear dynamics of phase separation in thin films. Nonlinearity **23**, 1559–1583 (2010)

[90] Net, M., Sánchez, J.: Continuation of bifurcations of periodic orbits for large-scale systems. SIAM J. Appl. Dyn. Syst. **14**(2), 674–698 (2015)

[91] Nicolaenko, B., Scheurer, B., Temam, R.: Some global dynamical properties of the Kuramoto-Sivashinsky equations: nonlinear stability and attractors. Physica D **16**(2), 155–183 (1985)

[92] Novick-Cohen, A.: The nonlinear Cahn - Hilliard equation: Transition from spinodal decomposition to nucleation behavior. J. Stat. Phys. **38**, 707–723 (1985)

[93] Novick-Cohen, A., Peletier, L.: Steady-states of the one-dimensional Cahn-Hilliard equation. Proc. R. Soc. Edinb. Sect. A-Math. **123**, 1071–1098 (1993)

[94] Oron, A., Davis, S.H., Bankoff, S.G.: Long-scale evolution of thin liquid films. Rev. Mod. Phys. **69**, 931–980 (1997)

[95] Oza, A., Heidenreich, S., Dunkel, J.: Generalized swift-hohenberg models for dense active suspensions. Eur. Phys. J. E **39**, 97 (2016)

[96] Pismen, L.M., Pomeau, Y.: Disjoining potential and spreading of thin liquid layers in the diffuse interface model coupled to hydrodynamics. Phys. Rev. E **62**, 2480–2492 (2000)

[97] Pismen, L.M., Thiele, U.: Asymptotic theory for a moving droplet driven by a wettability gradient. Phys. Fluids **18**, 042,104 (2006)

[98] Pomeau, Y., Zaleski, S.: The Kuramoto-Sivashinsky equation: a caricature of hydrodynamic turbulence? In: U. Frisch, J. Keller, G. Papanicolaou, O. Pironneau (eds.) Macroscopic modelling of turbulent flows (Nice, 1984), *Lecture Notes in Phys.*, vol. 230, pp. 296–303. Springer, Berlin (1985)

[99] Pototsky, A., Archer, A.J., Savel'ev, S.E., Thiele, U., Marchesoni, F.: Ratcheting of driven attracting colloidal particles: Temporal density oscillations and current multiplicity. Phys. Rev. E **83**, 061,401 (2011)

[100] Pototsky, A., Thiele, U., Archer, A.: Coarsening modes of clusters of aggregating particles. Phys. Rev. E **89**, 032,144 (2014)

[101] van Saarloos, W.: Front propagation into unstable states: Marginal stability as a dynamical mechanism for velocity selection. Phys. Rev. A **37**, 211–229 (1988)

[102] Sakaguchi, H., Brand, H.R.: Stable localized solutions of arbitrary length for the quintic Swift-Hohenberg equation. Physica D **97**, 274–285 (1996)

[103] Salinger, A.: LOCA (2016). `www.cs.sandia.gov/LOCA/` (last accessed 02/25/18)

[104] Sánchez, J., Garcia, F., Net, M.: Computation of azimuthal waves and their stability in thermal convection in rotating spherical shells with application to the study of a double-hopf bifurcation. Phys. Rev. E p. 033014 (2013)

[105] Sánchez, J., Net, M.: Numerical continuation methods for large-scale dissipative dynamical systems. Eur. Phys. J. Special Topics **225**, 2465–2486 (2016)

[106] Schelte, C., Javaloyes, J., Gurevich, S.V.: Dynamics of temporal localized states in passively mode-locked semiconductor lasers. Phys. Rev. A **97**, 053,820 (2018)

[107] Schüler, D., Alonso, S., Torcini, A., Bär, M.: Spatio-temporal dynamics induced by competing instabilities in two asymmetrically coupled nonlinear evolution equations. Chaos **24**, 043,142 (2014)

[108] Seydel, R.: Practical bifurcation and stability analysis. 3rd ed. Springer (2010)

[109] Sharma, A., Jameel, A.: Stability of thin polar films on non-wettable substrates. J. Chem. Soc. Faraday Trans. **90**, 625–627 (1994)

[110] Siero, E., Doelman, A., Eppinga, M.B., Rademacher, J.D.M., Rietkerk, M., Siteur, K.: Striped pattern selection by advective reaction-diffusion systems: resilience of banded vegetation on slopes. Chaos **25**(3) (2015)

[111] Sivashinsky, G.: Nonlinear analysis of hydrodynamic instability in laminar flames. I - Derivation of basic equations. Acta Astronautica **4**, 1177–1206 (1977)

[112] Snoeijer, J.H., Le Grand-Piteira, N., Limat, L., Stone, H.A., Eggers, J.: Cornered drops and rivulets. Phys. Fluids **19**, 042,104 (2007)

[113] Snoeijer, J.H., Ziegler, J., Andreotti, B., Fermigier, M., Eggers, J.: Thick films of viscous fluid coating a plate withdrawn from a liquid reservoir. Phys. Rev. Lett. **100**, 244,502 (2008)

[114] Sonnet, A., Virga, E.: Dynamics of dissipative ordered fluids. Phys. Rev. E **64**, 031,705 (2001)

[115] Spratte, K., Chi, L.F., Riegler, H.: Physisorption instabilities during dynamic Langmuir wetting. Europhys. Lett. **25**, 211–217 (1994)

[116] Stenhammar, J., Tiribocchi, A., Allen, R., Marenduzzo, D., Cates, M.: Continuum theory of phase separation kinetics for active brownian particles. Phys. Rev. Lett. **111**, 145,702 (2013)

[117] Swift, J., Hohenberg, P.C.: Hydrodynamic fluctuations at convective instability. Phys. Rev. A **15**, 319–328 (1977)

[118] Thiele, U.: Open questions and promising new fields in dewetting. Eur. Phys. J. E **12**, 409–416 (2003)

[119] Thiele, U.: Structure formation in thin liquid films. In: S. Kalliadasis, U. Thiele (eds.) Thin Films of Soft Matter, pp. 25–93. Springer, Wien (2007)

[120] Thiele, U.: Thin film evolution equations from (evaporating) dewetting liquid layers to epitaxial growth. J. Phys. Condens. Matter **22**, 084,019 (2010)

[121] Thiele, U.: Patterned deposition at moving contact line. Adv. Colloid Interface Sci. **206**, 399–413 (2014)

[122] Thiele, U., Archer, A., Pismen, L.: Gradient dynamics models for liquid films with soluble surfactant. Phys. Rev. Fluids **1**, 083,903 (2016)

[123] Thiele, U., Archer, A.J., Robbins, M.J., Gomez, H., Knobloch, E.: Localized states in the conserved swift-hohenberg equation with cubic nonlinearity. Phys. Rev. E **87**, 042,915 (2013)

[124] Thiele, U., Brusch, L., Bestehorn, M., Bär, M.: Modelling thin-film dewetting on structured substrates and templates: Bifurcation analysis and numerical simulations. Eur. Phys. J. E **11**, 255–271 (2003)

[125] Thiele, U., Madruga, S., Frastia, L.: Decomposition driven interface evolution for layers of binary mixtures: I. Model derivation and stratified base states. Phys. Fluids **19**, 122,106 (2007)

[126] Thiele, U., Velarde, M.G., Neuffer, K.: Dewetting: Film rupture by nucleation in the spinodal regime. Phys. Rev. Lett. **87**, 016,104 (2001)

[127] Toth, G., Tegze, G., Pusztai, T., Toth, G., Granasy, L.: Polymorphism, crystal nucleation and growth in the phase-field crystal model in 2d and 3d. J. Phys. Condens. Matter **22**, 364,101 (2010)

[128] Tseluiko, D., Galvagno, M., Thiele, U.: Collapsed heteroclinic snaking near a heteroclinic chain in dragged meniscus problems. Eur. Phys. J. E **37**, 33 (2014)

[129] Uecker, H.: Optimal harvesting and spatial patterns in a semi arid vegetation system. Nat. Resour. Model. **29**(2), 229–258 (2016)

[130] Uecker, H.: User guide on Hopf bifurcation and time periodic orbits with pde2path (2017). Available at [131]

[131] Uecker, H.: `www.staff.uni-oldenburg.de/hannes.uecker/pde2path` (last accessed 02/25/18) (2017)

[132] Uecker, H.: Hopf bifurcation and time periodic orbits with pde2path – algorithms and applications. Comm. in Comp. Phys. (to appear) (2018)

[133] Uecker, H.: Steady bifurcations of higher multiplicity in pde2path, preprint (2018)

[134] Uecker, H., Wetzel, D.: Numerical results for snaking of patterns over patterns in some 2D Selkov-Schnakenberg Reaction-Diffusion systems. SIADS **13-1**, 94–128 (2014)

[135] Uecker, H., Wetzel, D., Rademacher, J.: pde2path – a Matlab package for continuation and bifurcation in 2D elliptic systems. NMTMA **7**, 58–106 (2014)

[136] Wetzel, D.: Pattern analysis in a benthic bacteria-nutrient system. Math. Biosci. Eng. **13**(2), 303–332 (2016)

[137] Wilczek, M., Tewes, W., Engelnkemper, S., Gurevich, S.V., Thiele, U.: Sliding drops - ensemble statistics from single drop bifurcations. Phys. Rev. Lett. **119**, 204,501 (2017)

[138] Wilczek, M., Tewes, W.B.H., Gurevich, S.V., Köpf, M.H., Chi, L., Thiele, U.: Modelling pattern formation in dip-coating experiments. Math. Model. Nat. Phenom. **10**, 44–60 (2015)

[139] Wilczek, M., Zhu, J., Chi, L., Thiele, U., Gurevich, S.V.: Dip-coating with prestructured substrates: transfer of simple liquids and Langmuir-Blodgett monolayers. J. Phys. Condens. Matter **29**, 014,002 (2017)

[140] Wittkowski, R., Tiribocchi, A., Stenhammar, J., Allen, R., Marenduzzo, D., Cates, M.: Scalar phi(4) field theory for active-particle phase separation. Nat. Commun. **5**, 4351 (2014)

[141] Yin, H., Sibley, D., Thiele, U., Archer, A.: Films, layers and droplets: The effect of near-wall fluid structure on spreading dynamics. Phys. Rev. E **95**, 023,104 (2017)

[142] Zaks, M., Podolny, A., Nepomnyashchy, A., Golovin, A.: Periodic stationary patterns governed by a convective cahn-hilliard equation. SIAM J. Appl. Math. **66**, 700–720 (2006)

[143] Zelnik, Y., Uecker, H., Feudel, U., Meron, E.: Desertification by front propagation? J. Theor. Biol. pp. 27–35 (2017)

[144] Zhelyazov, D., Han-Kwan, D., Rademacher, J.D.M.: Global stability and local bifurcations in a two-fluid model for tokamak plasma. SIAM J. Appl. Dyn. Syst. **14**, 730–763 (2015)

[145] Ziegler, J., Snoeijer, J., Eggers, J.: Film transitions of receding contact lines. Eur. Phys. J.-Spec. Top. **166**, 177–180 (2009)